Tutor/s

Dr. Xavier Giménez Font
Departament de Ciència de Materials i Física Química

Dr. Hèctor Prats Garcia
Departament de Ciència de Materials i Física Química

Màster en Enginyeria Química

Treball Final de Màster

Computational evaluation of Ni-MOF-74 for the industrial separation of CO_2.
Avaluació computacional del Ni-MOF-74 per la separació industrial de CO_2.

Catalina Dupuy Pol

(June 2019)

UNIVERSITAT DE BARCELONA

Dos campus d'excel·lència internacional
B:KC Barcelona Knowledge Campus
HUB Health Universitat de Barcelona Campus

En primer lloc, donar gràcies als meus tutors Dr. Héctor Prats i Dr. Xavier Giménez per donar-me l'oportunitat de formar part d'aquesta investigació i per la dedicació interminable. Gràcies també a cada professor que m'ha fet créixer, tant professionalment com personalment, i que m'ha fet valorar l'educació. A la meva família, agrair el suport incondicional i la confiança cega que em brinden dia a dia, així com l'oportunitat d'estudiar fora. Al Sergio, gràcies pels ànims incansables i per fer que senti casa meva prop. Fer menció als companys del màster, per l'aprenentatge conjunt. Finalment, als amics que fan que el camí sigui més fàcil i han estat imprescindibles durant aquests anys.

Report

CONTENTS

1. SUMMARY

The exponential increase in energy consumption caused by population growth and industrial development has led to an increase in CO_2 emissions. Therefore, CO_2 has become the main greenhouse gas, which has raised a great concern in society. Reduction or elimination of these emissions can be carried out by adsorbent materials capable of selectively capturing this compound at the main source. One of these promising materials are the metal organic frameworks (MOF).

This project is based on the study of one of these MOF, specifically the Ni-MOF-74, for the separation of CO_2 in industrial mixtures, such as post-combustion, biogas and syngas mixtures. In addition, the effect of SO_2 impurities in the post-combustion mixture has been studied, since it is a competitor compound in adsorption process. Finally, the most suitable process and its optimum operating conditions has been selected for each mixture.

To develop this work, computational simulations have been carried out with the Grand Canonical Monte Carlo method (GCCM), which allows to obtain adsorption isotherms and isobars by means of validated force fields.

Keywords: CO_2 emissions, capture, metal organic frameworks (MOF), adsorption.

2. INTRODUCTION

Population growth and industrial development in the 21st century has led to an exponential increase in energy consumption. This energy mainly comes from fossil fuels (85%) and these are responsible for 40% of CO_2 emissions into the atmosphere [1]. CO_2 emissions have increased significantly due to these factors, thus becoming the main anthropogenic greenhouse gas. Approximately 60% of the effects of global warming are attributed to CO_2 emissions [2].

There are three options for reducing these emissions: improving efficiency to reduce energy use, using non-fossil fuels such as renewable energy to reduce carbon intensity or improve CO_2 capture and sequestration by developing new technologies [1].

One of the best options is the capture and sequestration of CO_2 (CCS), hence many investigations carry out improvements in existing technologies or new technologies of CCS [1], although the objective should be the capture, sequestration and use of carbon (CCSU), that would allow to achieve a society supplied by clean energy through the revaluation of CO_2.

These investigations suggest that the process of adsorption with porous solids is more energy efficient than adsorption with liquids, which is the traditional way. In addition, good candidates as solid adsorbents are the metal organic frameworks (MOF) which are crystalline materials formed by metal ions bonded by an organic part. One of the best-known MOF families is M-MOF-74 (M-CPO-27 or M/DOBDC) which is formed by transition metals of the first row (M = Mg, Fe, Co, Ni, Cu or Zn) connected by linkers 2,5-dioxide-1,4-benzenedicarboxylate for the formation of one-dimensional hexagonal channels. These MOF have a great interaction with CO_2, while the affinity is weak towards other components present in industrial gas mixtures, such as N_2, H_2 and CH_4.

The most studied MOF in this family is Mg-MOF-74, which stands out for its CO_2 adsorption capacity. However, in this project the Ni-MOF-74 is studied due to its greater desorption [2]. Moreover, in the Swing Adsorption Processes (SAP) a key step is the regeneration of the material. Therefore, this project consists in the determination of the most suitable SAP and its optimal conditions for the separation of CO_2. To perform the

study, results are obtained from computational simulations using the Monte Carlo method, which allow to simulate the process reality through parameters involved in it and thus avoid experimental work.

The mixtures of gases studied are the common ones in the production of electrical energy: post-combustion mixture, biogas and syngas. On the other hand, the three SAP considered are Pressure Swing Adsorption (PSA), Vacuum Swing Adsorption (VSA), and Temperature Swing Adsorption (TSA).

3. OBJECTIVES

The main objective of this project is the evaluation of Ni-MOF-74 for CO_2 capture in post-combustion mixture, biogas and syngas, which are gas mixture industrial streams.

To achieve this objective, concrete aims are established:

- Perform Grand Canonical Monte Carlo simulations to obtain all the adsorption data at different operating conditions.
- Calculate several adsorbent evaluation criteria for Ni-MOF-74 operating under three different Swing Adsorption Processes (PSA, VSA and TSA).
- Find the optimal operating conditions for CO_2 separation in those Swing Adsorption processes: compromise between high working capacity and low energy index.
- Study the effect of impurities (SO_2) in the post-combustion mixture for CO_2 separation.

4. FUNDAMENTALS

The main aim of this chapter is to provide an introduction to CO_2 capture by solid adsorbents, as well as a brief explanation of the methodology used to compute the adsorption data.

4.1. CO_2 capture technologies

Reduction of carbon dioxide emissions in the atmosphere can be carried out in different ways: increasing the efficiency of combustion processes, using biofuels and renewable energies, or using CCS technologies [1].

Some of the most used technologies are the following [2]:

- Chemical absorption with amines: it is currently the most popular technology, being based on the room temperature exothermic reaction of a sorbent with the carbon dioxide present in the gaseous stream [3]. Among the amines, the most currently used in industry is monoethanolamine [4]. This process has some disadvantages such as the need of high energy to regenerate the amines and the degradation caused by the presence of O_2, SO_2, NO_2 and HCl [3, 4] in the gas stream.
- Cryogenic distillation: first, N_2 and CO_2 are sent to a cryogenic chamber. Next, CO_2 is condensed at the appropriate temperature and pressure, while N_2 remains as a gas. The main advantage is that liquid CO_2 is obtained, which can be transported and/or stored. The shortcoming of this approach is that it requires a large amount of energy, rendering it low–performing in economic terms [5].
- Membrane-based separation: membranes are similar to filters and their separation mechanism is determined by solution-diffusion, adsorption-diffusion, molecular sieve, and ion transport processes at the molecular level [6]. Flue mixture is passed through a membrane and the CO_2 separation is generally due to partial pressure difference of CO_2 across the membrane or reversible chemical reaction with carriers or porous inorganic materials. This type of separation has been quite used industrially, but it is still in the research development phase and, furthermore, it presents instability at reforming environment stages [2].

- Biological methods: these processes consist of CO_2 fixation by microorganisms, such as cyanobacteria and microalgae [1].

The main shortcoming of the previous technologies is their high energy cost. According to United States' Department of Energy and National Energy Technology Laboratory, it is required a technology that captures 90% of CO_2 without raising the cost more than 35% in electricity [7]. Therefore, new cost-efficient alternatives that can satisfy these conditions are needed. One of them is the adsorption process on the pores of solid materials, like activated carbons, zeolites or metal organic frameworks (MOF). This step might be accomplished through specific Swing Adsorption processes, such as Pressure Swing Adsorption (PSA), Vacuum Swing Adsorption (VSA), or Temperature Swing Adsorption (TSA). When used in combination with good solid adsorbents, such technologies may provide lower regeneration energy, higher working capacity and selectivity, and ease of handling.

The present work focuses on this approach, which will be described in more detail below.

4.2. Adsorption

Adsorption is a separation process of liquid or gaseous mixtures by a support, generally a porous solid material, becoming an interfacial layer between the two resulting phases. In this process, one or more constituents of the mixture (atoms, ions or molecules) are retained on the surface of the solid [8], the separation arising from unbalanced residual forces at the solid surface. Therefore, the separated amount is related to the balance between the adsorbent and the adsorbate and it depends on their nature and the operating conditions. In general, the porous solid surface displays active centres, which are able to create bonds with the liquid or gaseous phase molecules upon contacting them [9,10]. The forces responsible for the adsorption are van der Waals and electrostatic. Van der Waals forces are weak and are related to the adsorbate molecular polarizability, whereas the electrostatic forces are due to the attraction of charges of opposite sign [11]. Continuous, efficient operation requires the porous solid material

recovery. Adsorbate species can be desorbed by reducing the pressure or increasing the temperature. This step is called adsorbent regeneration [10].

As pointed out above, one may distinguish two different types of adsorption processes, at the molecular level [12]:

- Physical adsorption: the adsorbed species are weakly attached (ca. 10–40 kJ/mol of binding energy) to the surface, thanks to dipole-dipole and dipole-induced interactions, and maintains its molecular integrity [12].
- Chemical adsorption: stronger chemical bonds (between 100 and 800 kJ/mol) are formed between the adsorbate and the surface atoms. These interactions can be ionic or covalent [12, 13], even involving electron transfer between the adsorbate and the adsorbent.

Table 1 details some of the main differences between chemical adsorption and physical adsorption [12].

Table 1. Main differences between chemical and physical adsorption.

PROPERTIES	PHYSICAL ADSORPTION	CHEMICAL ADSORPTION
Adsorbent	All solids	Some solids
Adsorbate	All gases below critical temperature	Some chemically reactive gases
Temperature range	At low temperatures (≈ adsorbate boiling point)	Usually, at high temperatures (greater than adsorbate boiling point)
Adsorption enthalpy	Low: -ΔH ≤ 20 kJ/mol	High: -ΔH ≈ 50-300 kJ/mol
Velocity, activation energy E	Very fast, E very small	Activated, high E Not activated, E small
Pressure effect	Strong	Weak
Covering	Monolayer-multilayer	Monolayer
Desorption	Easy in vacuum or by action of a purge gas	Desorption Eact > 50-100 kJ/mol. It occurs at high temperatures
Reversibility	Extremely reversible	Often, irreversible

4.3. Adsorption isotherms

The most commonly used characterization for the adsorption process is by means of the adsorption isotherm, i.e. the relationship between the equilibrium adsorbed amount and pressure, at constant temperature, as its name suggests. The adsorbate amount is expressed as adsorbent mass or volume, as a function of pressure. It is a way to evidence the change in adsorbent species quantity, as pressure is increased.

The study of adsorption isotherms provides valuable information: surface area/pore volume ratios, pore size distribution, and adsorbent chemical surface composition, among others. IUPAC classifies adsorption isotherms into six types, according to their shape as a function of pressure. This classification is shown in the following figure (Figure 1) [14]:

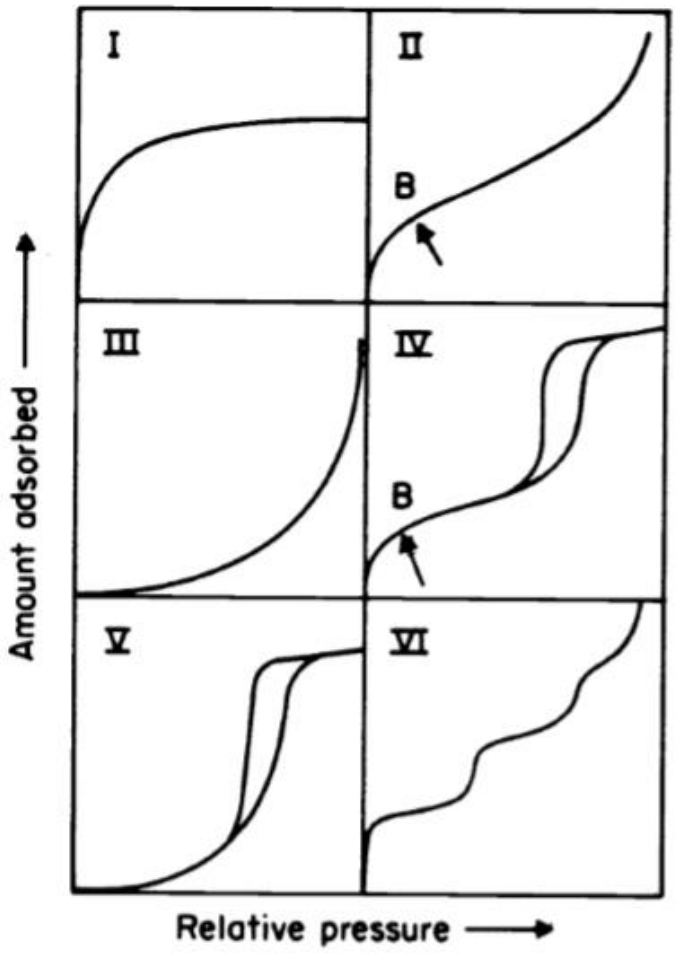

Figure 1. Adsorption isotherms classification according to IUPAC.

Each of the curve shapes ultimately provides information on the interactions between the adsorbate and the adsorbent.

Concerning pore size distribution, IUPAC distinguishes three types of porous solids, depending on the most frequent pore size: *microporous*, *mesoporous* and macroporous. Microporous have diameters of less than 2 nm and are able to adsorb small molecules, while mesoporous adsorb large molecules since they have a diameter between 2 and 50 nm. On the other hand, macroporous have diameters above 50 nm, and usually act as support for small pore materials to improve their function [14]. In this regard, isotherms may change with adsorbent pore sizes: medium-high pressures are required in mesoporous materials to feature adsorption, whereas microporous adsorbents evidence adsorption already at low pressures.

Next, the six types of isotherms are further described [14, 15]:

Type I isotherms are typical of microporous adsorbents,. This isotherm features a sudden, fast increase in adsorbed gas, at low pressures, until it reaches a maximum and remains constant. The existence of this saturation value is the pore size, since it limits the adsorption flux. This limiting flux causes also that adsorption occurs in monolayers. This isotherm is also known as Langmuir isotherm, being the most common in active carbons and zeolites.

Type II isotherms are given by non-porous or macroporous adsorbents and their shape is due to multilayer adsorption. The first saturation region shows the pressure at which the monolayer adsorption is complete and multilayer adsorption begins. After this point, the amount adsorbed increases with rising pressure.

Type III isotherms appear in macroporous or non-porous materials, when there is little affinity between adsorbent and adsorbate. At low pressures, the formation of weak interactions between adsorbent and adsorbate do not produce complete adsorption, although at high pressures the interactions strength between them increases significantly the amount adsorbed.

Type IV isotherms take place in mesoporous solids and are determined by hysteresis cycles, which are associated with pore capillary condensation. At relatively low pressures, it is similar to type II isotherm, since monolayer adsorption occurs. But as the

pressure increases, multilayer adsorption and capillary condensation appear. This phenomenon causes the desorption that is directly related to the hysteresis loop.

On the other hand, type V isotherms represent mesoporous adsorbent processes, in which adsorbate and adsorbent interactions are weak and there is presence of hysteresis. Consequently, it can be explained as a mixture between type III and type IV isotherms. This shape is rare to find.

Finally, the type VI isotherms evidence layer by layer adsorption processes, in a stepped mode. Thus, there is a sequential adsorption in multilayer on non-porous solids. It is not a common isotherm, an example being some noble gas adsorption processes on uniform surfaces.

4.4. Adsorbent evaluation criteria

The performance of a given adsorbent under different operating conditions can be evaluated by measuring, or computing, parameters like isosteric heat of adsorption, uptake, selectivity, working capacity, purity and energetic cost.

4.4.1. Isosteric heat of adsorption

The isosteric heat of adsorption (q_{st}) measures the interaction strength between adsorbent and adsorbate. This parameter indicates the energy released during the adsorption process and can be calculated from the Clausius-Clapeyron equation for adsorption equilibrium [13]:

$$q_{st} = -R \left. \frac{\partial \, ln \, P}{\partial \left(\frac{1}{T}\right)} \right]_N = R \, T^2 \left. \frac{\partial \, ln \, P}{\partial T} \right]_N \quad (1)$$

The higher the isosteric heat of adsorption, the more expensive will be the adsorbent regeneration step. However, low values may result in poor uptake and selectivity.

Physical adsorption processes have an isosteric heat of between 20 and 70 kJ/mol. On the other hand, the isosteric heat of chemical adsorption usually reaches higher values, above 80 kJ/mol, because the interactions are much stronger [13].

The isosteric heat of adsorption can be calculated, from GCMC, as energy/particle fluctuations:

$$-q_{st} = \frac{< U \times N > - < U > \times < N >}{< N^2 > - < N >^2} - < U_g > - R\,T \qquad (2)$$

Where U is the total potential energy of the system, N is the number of adsorbed molecules and Ug is the energy of an isolated single molecule. The brackets <> denote an average in the GC ensemble.

4.4.2. Uptake

The uptake is the amount of gas molecules adsorbed at a certain pressure and temperature, and it is usually expressed as mass uptake (moles of species A adsorbed per kilogram of adsorbent).

4.4.3. Selectivity

Selectivity is the capacity to separate a desired component from the mixture. The selectivity is influenced by the adsorbate-adsorbent interactions, the differences in size and shape of the fluid phase components, and the differences in the diffusion rates of the molecules through the pores.

The selectivity of component 1 relative to component 2 can be calculated as [16]:

$$S_{\frac{1}{2}} = \left(\frac{x_1}{x_2}\right)\left(\frac{y_2}{y_1}\right) \qquad (3)$$

Where x is the molar fraction in the adsorbed phase and y is the molar fraction in the fluid phase at feeding conditions.

4.4.4. Working capacity

The working capacity which is defined as the difference in the uptake under adsorption, $q_i^{mix}(P_{ads}, T_{ads})$, and desorption, $q_i^{mix}(P_{des}, T_{des})$, conditions: [16]

$$\begin{aligned} WC_i &= q_i^{mix}(P_{ads}, T_{ads}) - q_i^{mix}(P_{des}, T_{des}) \\ &\approx q_i^{mix}(P_{ads}, T_{ads}) - \phi_i \cdot q_i^{pure}(P_{des}, T_{des}) \end{aligned} \qquad (4)$$

The first term in Eq. (4) can be obtained directly from the mixture adsorption isotherm at adsorption conditions. On the other hand, the usual procedure of estimating $q_i^{mix}(P_{des}, T_{des})$ is to assume that this value is equal to the pure-component uptake of CO_2 at the desorption conditions. However, this procedure assumes that after the adsorption step the composition inside the bed is 100% CO_2, but in some case, there is a non-negligible fraction of other components adsorbed. Thus, a correction factor ϕ_i that ranges from 0 to 1 must be included which accounts for the molar fraction of CO_2 in the bed.

This criterion is generally more relevant than the total uptake at the adsorption pressure, since it really determines the amount of flue gas component that can be separated at each swing adsorption cycle. Ideally, all the adsorbate would be desorbed so the adsorbent would be fully regenerated. Then, the value of the working capacity would be equal to the adsorption uptake. In practice, however, some adsorbate molecules remain adsorbed after the desorption step. A compromise must be find between work capacity and required energy for the desorption step.

4.4.5. CO_2 purity

Another important parameter is CO_2 purity at outlet, especially if we want to reuse the CO_2 captured for other applications. It can be calculated as [17]:

$$X_{CO_2} = \frac{N_{CO_2}^{out}}{N_{gas}^{out}} = \frac{\frac{P_{CO_2} V \varepsilon}{RT} + WC_{CO_2} \rho V (1-\varepsilon)}{\frac{P_{TOT} V \varepsilon}{RT} + (\sum WC_i) \rho V (1-\varepsilon)} \quad (5)$$

The ratio $\frac{N_{CO_2}^{out}}{N_{gas}^{out}}$ indicates the molar fraction of CO_2 in the mixture exiting the adsorbent material and ε is the void fraction of the bed (void volume/total volume of the bed).

4.5. CO_2 adsorbents

Good candidates, to be used as solid adsorbent materials, must show high working capacity, purity and selectivity and low energetic cost. In addition, an ideal adsorbent must have adequate adsorption-desorption kinetics, be stable during the repetition of thousands of cycles, and must be cheap (i.e. less than 10 $ per kilogram) [2, 18]. Finally, another important feature is its stability in the presence of impurities such as SO_2 and NO_2.

In this section, some of the most promising adsorbents for CO_2 capture are described.

4.5.1. Activated carbons

Activated carbons are the most studied and industrially used materials in adsorption processes. These solids are composed of biological materials with carbon, industrial by-products and/or biomass [19]. Therefore, one of its advantages is the low cost of raw materials. In addition, the variety of raw materials provides a wide distribution of pore size and active surface area.

Other advantages of activated carbons are thermal stability and hydrophobic character. Thermal stability allows to work at high temperatures and hydrophobic character to maintain the adequate performance in the presence of H_2O, which is one of the main impurities that causes deactivation of materials [19]. Also, there are disadvantages such as low adsorption capacities at low temperatures and the need to work at high pressures to reach high capacities.

The two elementary phases to produce activated carbons are carbonization and activation. In this last step, adequate porosity and, consequently, active sites are provided [19].

Figure 2. Activated Carbon
(RaveDave, 06/06/19 via Wikipedia Commons, Creative Commoms Attribution)

4.5.2. Zeolites

Zeolites are microporous aluminosilicate solids, used commercially for adsorption and catalysis. These materials are composed by aluminium, oxygen, silica and alkaline or alkaline-earth metals. More specifically, AlO_2 and SiO_2 form tetrahedra that share edges (oxygen atoms). In this way, silica and aluminium are in the centre, while oxygen atoms are at vertices. These tetrahedral structures are repeated in the three dimensions forming solids of different configuration [12].

Some zeolites are from natural origin and many others are obtained in the laboratory by crystallization processes [12]. They are one of the most studied materials for CO_2 capture in post-combustion flue gas because high pressure operation is not needed. In addition, zeolites have a high chemical and thermal stability. One should note, however, that the presence of water in post-combustion gases causes a substantial decrease in adsorption capacity due to its hydrophilic character.

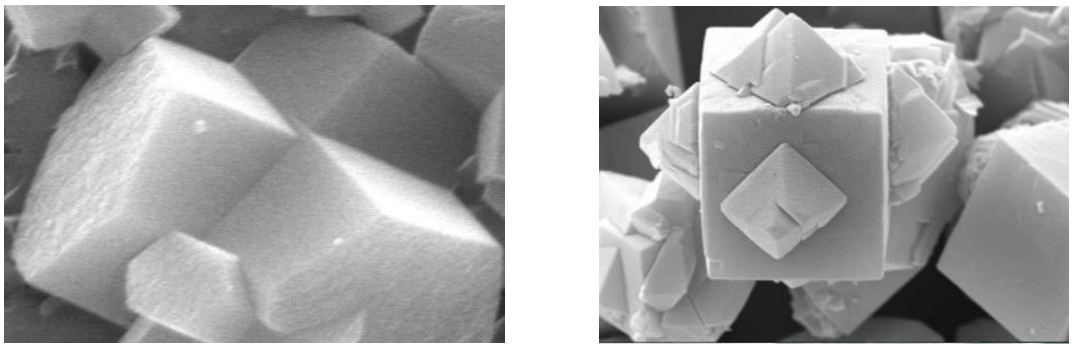

Figure 3. Zeolites
(taken from [12])

4.5.3. Metal-Organic Frameworks

In the last decade, many porous materials have been synthesized for its use as adsorbents. One family of materials are the Metal Organic Frameworks (MOFs), which are among the most promising [20].

MOFs are inorganic and organic hybrid materials, composed of metal atoms linked by organic ligands through coordination bonds. The coordination bonds strength provides a crystalline form [20]. These porous solids may show up great diversity, featuring robustness (permanent porosity), high surface area, thermal and chemical stability, high

pore volume and low density [2]. Therefore, its functionality and design allow MOF to be good candidates for adsorption, storage, separation and catalysis [20].

MOF design can occur by modifying the way in which they join to form the crystalline structure, which is called reticular or modular synthesis. Hence, it is possible to optimize its structure for specific applications: structure of pores, surface functional groups, among other properties. In addition, these materials present high working capacities compared to other materials such as zeolites [2, 20].

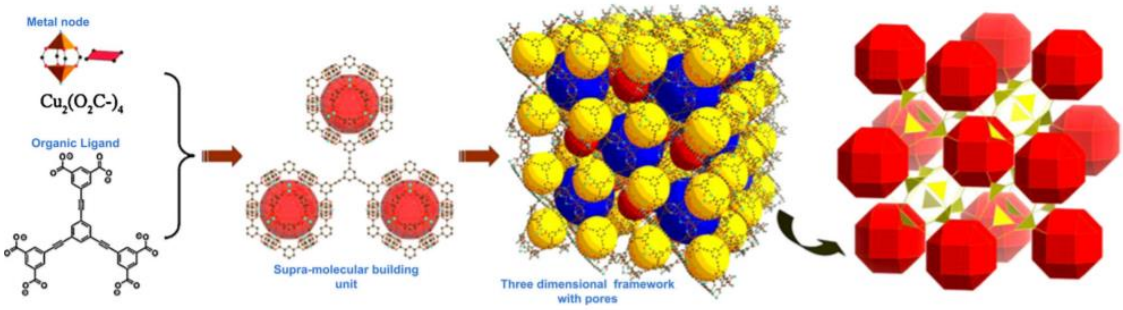

Figure 4. Modular synthesis of MOF.

(taken from: [2])

Gas separation and purification by means of MOFs is one of the most active research lines, since it offers advantages due to its structural characteristics. There is still, however, a long way to go, since this research is in their initial stage [20].

One of the most studied MOF families is M-MOF-74, also known as M-CPO-27 or M/DOBDC. These MOFs are constituted by metal bonds formed after elimination of metal atoms axial ligand, which can be carried out by thermal activation. They have an advantage over other MOFs, since they can have unsaturated coordinated metallic sites that can be modified without affecting the framework structure [21].

The structure of M-MOF-74 is shown in figure 5, which consists of carbon atoms (gray), oxygen atoms (red) and metal atoms, which may be either Mg, Ni, Co or Zn (blue).

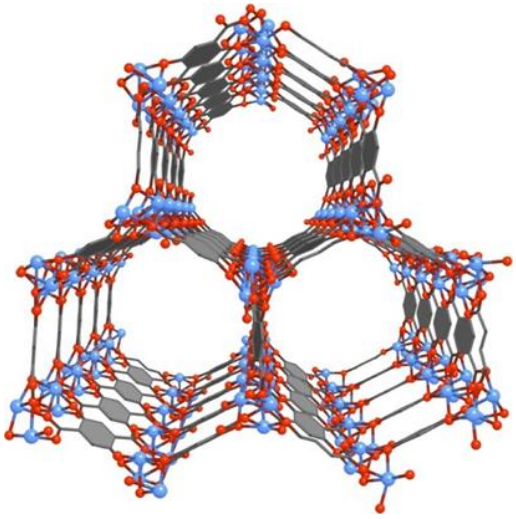

Figure 5. M-MOF-74 structure.
(taken from: ref [22])

The aim of this work is to study CO_2 adsorption, i.e. capture and separation from industrial gas mixtures through the Ni-MOF-74. The synthesis of this MOF is carried out by a hexagonal packing of helical O_5Ni chains connected by 2,5-dihydroxyteraphthallate linkers [22]. Ni-MOF-74 is a microporous material with pore radius of about 7-8 nm, high stability and high CO_2 capacity [23]. On the other hand, it has a hydrophilic character that provides affinity to H_2O, saturating the material and decreasing its separation performance. In dry conditions, Ni-MOF-74 can retain up to 60% of its initial capacity. Thus, in this study it is assumed that all gas mixtures have passed through a water filter before the adsorption process [24].

The structure of Ni-MOF-74 is shown in more detail in Figure 6, where carbon is gray, oxygen is red, hydrogen is white, and nickel is blue.

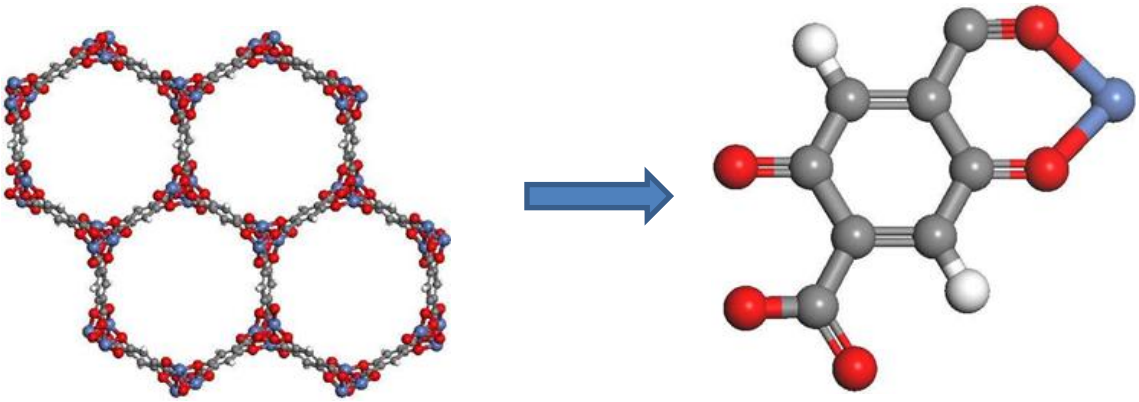

Figure 6.Molecular structure of Ni-MOF-74 and organic linker connected to Ni.
(taken from: [22])

4.6. Technologies for CO_2 capture at industrial level

CO_2 capture process is focused on one point in the industrial process. Thereby, according to the carbon dioxide separation point, there are three technologies [3]:

- Pre-combustion capture
- Post-combustion capture
- Oxycombustion capture

Pre-combustion capture is based on decarbonization of fuel before combustion, which reacts with oxygen or air (gasification) and produces a high-pressure combustion gas formed mainly by carbon dioxide and hydrogen (syngas). Also, the separation is easier due to a higher concentration and partial pressure of CO_2. This technology offers advantages such as lower energy cost than post-combustion capture and smaller separation equipment. In addition, hydrogen separated from CO_2 is used for energy generation [3, 25].

On the other hand, post-combustion capture consists in the separation of the CO_2 from products of the combustion reaction before releasing them to the atmosphere. It is a method that involves a higher level of complexity due to the low concentration and partial pressure of CO_2 and the high temperature of the post-combustion mixture.

Finally, in the oxy-combustion process, the air is substituted by pure oxygen. This implies that the post-combustion gases will be mainly carbon dioxide and water. Thus, by increasing the CO_2 concentration, the separation process is easier. This technique has a lower operating cost, although the main limitation for its application is given by high temperatures of the flame when it is used almost pure oxygen [25,26].

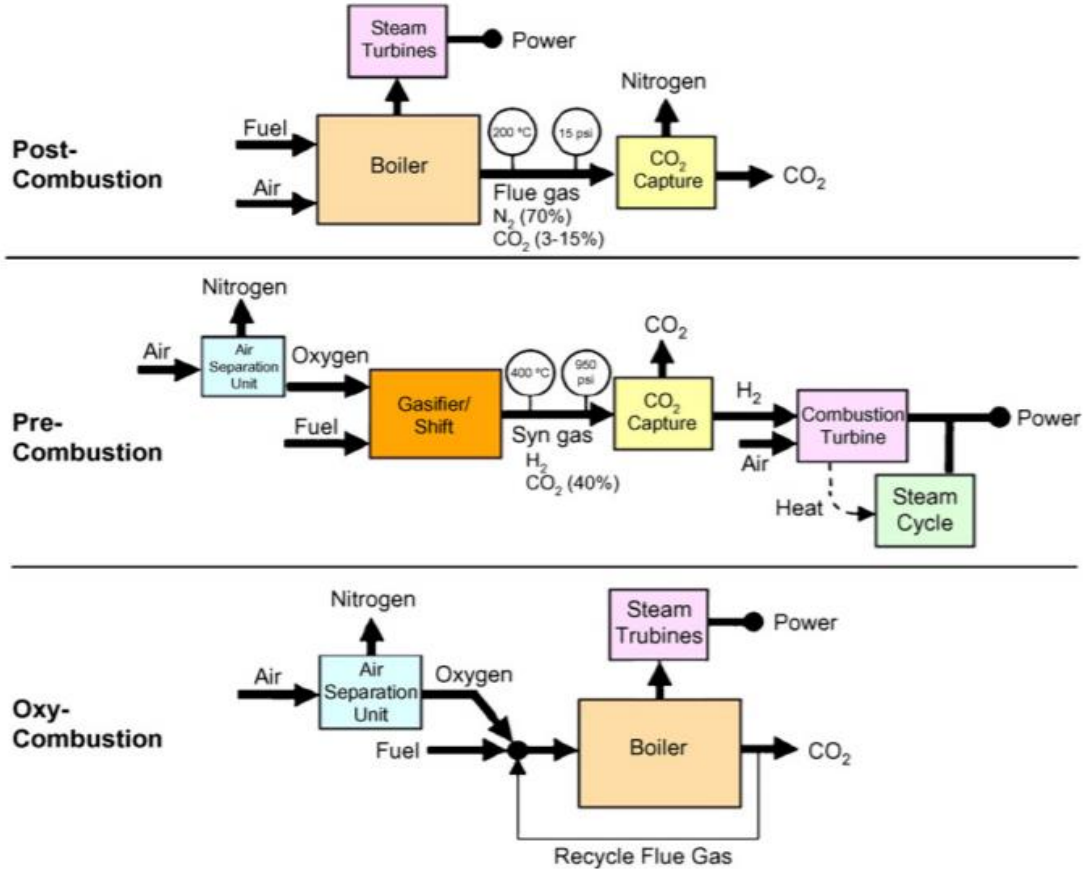

Figure 7. CO2 capture technologies at industrial level.
(Taken from ref [24])

4.7. Swing Adsorption Processes

The separation processes of CO_2 based on adsorption on solid materials require two stages: adsorption and desorption (also called adsorbent regeneration).

In SAP, a gas stream is introduced into the adsorber equipment and the outlet valve remains open for gas ventilation. When the bed is saturated, inlet and outlet valves are closed. Then, the adsorbed is regenerated by lowering the pressure or increasing the temperature. Since the adsorption process is discontinuous, usually at least two beds are used (Figure 8), in such a way that, while one bed is adsorbing, the other bed is desorbing. This allows to work in semi-continuous.

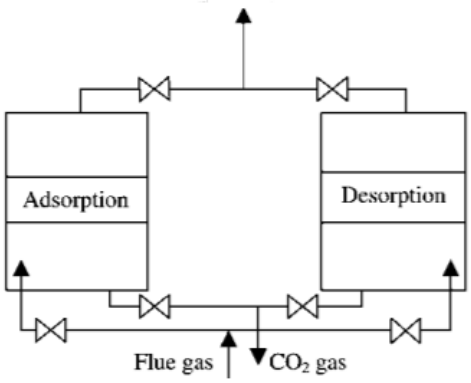

Figure 8. Swing Adsorption Process

(taken from [5])

There are three main types of Swing Adsorption Processes [27,28]:

- Temperature Swing Adsorption (TSA): This method consists of increasing the temperature for the regeneration of the adsorbent. Thus, desorption occurs at higher temperatures than adsorption. This is due to the instability of the CO2 molecules in the pores when they gain energy. When the cycle is finished, the temperature is reduced to begin the adsorption process again.
- Pressure Swing Adsorption (PSA): In this process, adsorption occurs at high pressures, while desorption at atmospheric pressure. The feed gases are pressurized before entering the adsorbent equipment. The greater the difference between the adsorption and desorption pressure, the greater the amount of CO2 is desorbed. The process of desorption is easy, since the pressure is atmospheric. On the other hand, adsorption, by requiring high pressures, is a very expensive process, especially in large quantities of gas.
- Vacuum Swing Adsorption (VSA): This process is similar to the previous one, but the adsorption step occurs at atmospheric pressure and the desorption at very low pressures, nearly vacuum. Then, the lower the desorption pressure, the more CO_2 is extracted.

The energy required to perform these processes depend on the chosen material and the operating conditions. Therefore, in this work the performance of Ni-MOF-74 on these three processes will be evaluated and the optimum operation conditions will be found.

4.8. Applications of CO_2

In food industry, CO_2 is used in carbonated beverages and to avoid wine oxidation when it matures. Furthermore, it is used in packaged products to inhibit bacteria growth: packaging in modified atmosphere (MAP) and packaging in controlled atmosphere (CAP). Supercritical CO_2 is the raw extracting solvent in the production of coffee and tea, beer hops and in cocoa fat [29]. Another important use is as a cryogenic agent in refrigeration and freezing processes. This gas is also used in the oil industry to reduce oil viscosity in Enhanced Oil Recovery processes (EOR) [30]. Another common application of CO_2 is in fire extinguishers and industrial fire protection systems (fire extinguishing technology), which reduces the level of oxygen necessary for combustion.

In chemical industry, it is used as raw material to increase production yield of chemical products, such as methanol, formaldehyde and urea (agricultural fertilizer) [31]. Moreover, it is consumed in wastewater treatment and in drinking water demineralization. It stands out as a refrigerant gas and as a pressurized gas.

Although there are applications for CO_2, emissions of this gas are much greater than its demand. Thus, the part that is not used should be stored. Geological storage is the most common, which is based on the confinement of CO_2 in a geological formation. This method consists of CO_2 injection, generally in deep zones, such as oil deposits or deep saline aquifers [32]. There are other methods of storage: biological storage and storage in oceans. Biological storage is carried out by terrestrial or marine ecosystems capable of absorbing atmospheric CO_2. Storage in oceans is still under study and involves injecting CO_2 into sea bottoms to isolate it from the atmosphere.

5. COMPUTATIONAL SIMULATIONS

Computational simulations allow us to study the performance of several adsorbent materials and screen a wide range of operating conditions, solving systems of differential equations by means of supercomputers.

The macroscopic properties of a system can be studied from its microscopic properties using statistical mechanics. The microscopic properties of interest are the position of all the particles in our system and the interactions between them.

In the context of statistical mechanics, an ensemble is defined as a collection of replicas of the system with different microscopic characteristics but sharing all macroscopic properties defining the ensemble. Depending on the conditions under which our thermodynamic system is, several ensembles can be defined. When simulating the adsorption process on a solid adsorbent, the number of molecules in the ensemble is not constant. Hence, this type of simulations are carried out in the Grand Canonical ensemble, where the fixed parameters are the volume, the temperature, and the chemical potential. Concretely, all the simulations performed in the present work have been carried out by means of the Grand Canonical Monte Carlo (GCMC) method. The details of this method will be explained below.

5.1. Force fields

The interactions between the different particles in the system can be calculated by classical methods, which consider molecules composed by a set of spheres (i.e., atoms) of different sizes and masses, connected by rigid or flexible bonds and governed by classical potential energy functions. As a direct consequence of this model, the total energy of a molecule is obtained as the sum of several contributions or perfectly defined terms that depend on the spatial coordinates of the nuclei. The functional form and parameter set used to calculate the potential energy of a system of atoms is referred as a force field (FF), since the derivatives of the potential energy function determine the forces on the atoms.

The total energy of the system can be divided into two main contributions: interactions between linked atoms and interactions between unbound atoms. In addition, each of these energies is divided in several contributions. The energy of the interactions

between bonded atoms comes from bond stretching forces, bond bend and dihedral torsion, while the energy of the interactions between unlinked atoms is given by van der Waals forces and electrostatic forces. Therefore, energy can be expressed by:

$$U_{total} = U_{bonded} + U_{non-bonded} \quad (6)$$

$$U_{bonded} = U_{bond} + U_{bend} + U_{torsion} \quad (7)$$

$$U_{non-bonded} = U_{Van\ der\ Waals} + U_{electrostatic} \quad (8)$$

These parameters can be obtained through adjustment with respect to experimental data, such as density, adsorption heat, vaporization heat, or adjustment of quantum studies parameters.

Interactions of unbonded atoms become important in the adsorption processes, since they are those present between the adsorbent and the adsorbate. As stated above, these interactions are van der Waals forces and electrostatic forces.

5.1.1. Van der Waals forces

Van der Waals forces depend on the distance between atoms or molecules quickly vanished at longer distances. These forces present attractive forces, due to instantaneous fluctuations of electrical dipoles moments, and repulsive forces, which are given from the penetration or superposition of the electronic cloud between molecules and adjacent surfaces. These forces are weak, so it is easy to disturb them. These interactions can be described by the 12-6 Lennard-Jones potential. [16, 17]:

$$U_{Van\ der\ Waals}(r_{ij}) = 4 \cdot \varepsilon \left[\left(\frac{\sigma}{r_{ij}} \right)^{12} - \left(\frac{\sigma}{r_{ij}} \right)^{6} \right] \quad (9)$$

Where ε is the depth of the potential well, which measures the force in which two particles attract each other, and σ is the distance at which the potential between particles is zero (Figure 9) [16, 17]. In addition, the term $1/r_{ij}^{12}$ describes the repulsion between atoms when they are close and postulates that when the electron clouds of

two atoms overlap energy grows abruptly (Pauli's principle). On the other hand, the term $1/r_{ij}^6$ describes the system cohesion, that is, the attractive forces.

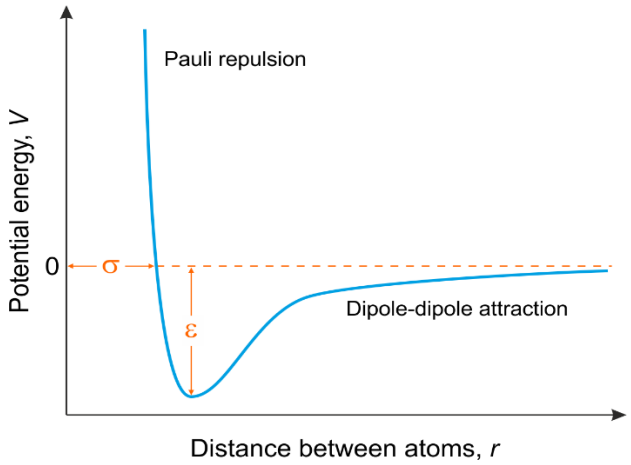

Figure 9. Lennard-Jones potential.
(taken from: E. Generalic, https://glossary.periodni.com/glossary.php?en=Lennard-Jones+potential, accessed 06/06/19)

This equation is combined with the Lorentz-Berhelot rules, which allow to describe interactions between different atoms [16,17].

$$\varepsilon_{ij} = \sqrt{\varepsilon_{ii} \cdot \varepsilon_{jj}} \tag{10}$$

$$\sigma_{ij} = \frac{\sigma_{ii} + \sigma_{jj}}{2} \tag{11}$$

5.1.2. Electrostatic forces

Electrostatic forces arise from the electric charges and follow the Coulomb's law:

$$U_{electrostatic}(r_{ij}) = \frac{1}{4 \cdot \pi \cdot \varepsilon_r \cdot \varepsilon_0} \cdot \frac{q_i \cdot q_j}{r_{ij}} \tag{12}$$

Where ε_0 is the vacuum permittivity and has a value of $8.85419 \cdot 10^{-12}$ $C^2 \cdot N^{-1} \cdot m^{-2}$, ε_r is the electric constant of the habitat where electric charges are assigned, q_i i q_j are the electric charges of the atoms and r_{ij} the distance between these atoms [16, 17].
These interactions are much stronger than van der Waals forces, and its calculation is more laborious. To calculate them, the Ewald sum method is used [33, 37].

5.2. Boundary conditions and potential truncation

The simulation occurs in a simulation cell. To perform it at microscopic level, it is necessary to apply boundary conditions to simulate an infinite environment of particles. For this, periodic boundary conditions are used, which from a primitive cell reproduces a periodic and infinite network of identical cells (Figure 10). Therefore, a particle interacts with both particles in its cell and particles of each replicated cell [38].

However, considering that all particles interact with each other, potential of each particle depends on the forces between all of them, so it is impossible to calculate it. Thus, since the potential is proportional to the distance between particles, it is stipulated that the potential only depends on nearby particles and distant particles are not significant. Likewise, a cut-off radius is established from which the interactions are not calculated, giving a value of zero to all the interactions between the particles that are outside that radius. The establishment of the cutting radius is named potential truncation.

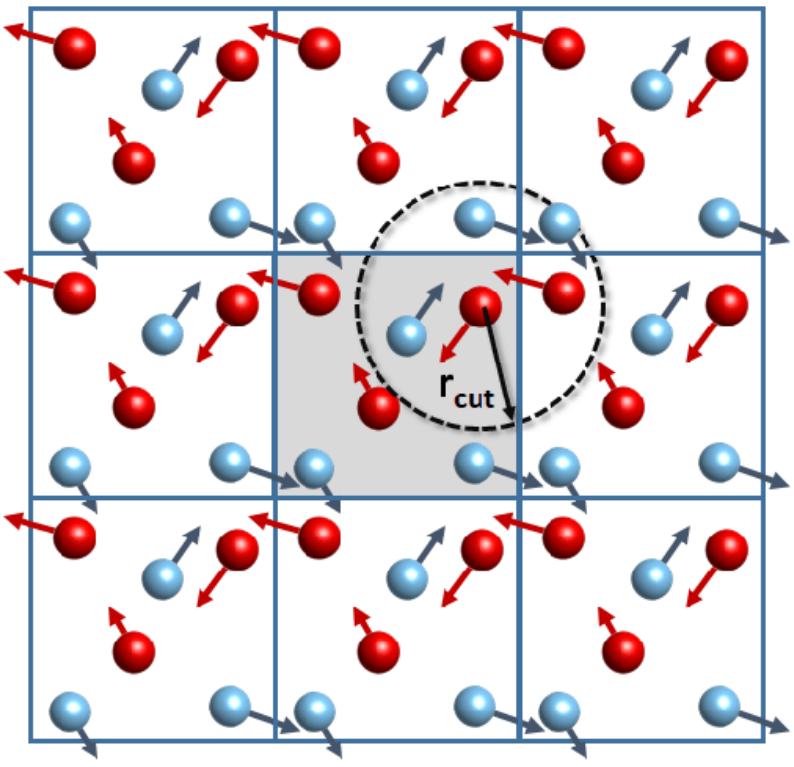

Figure 10. Periodic boundary conditions
.(taken from: Improving the Functional Control of Ferroelectrics using Insights from Atomistic modelling - Scientific Figure on ResearchGate. Available from: https://www.researchgate.net/figure/2D-representation-of-periodic-boundary-conditions-applied-to-a-cubic-principle-cell_fig18_328382488 [accessed 06/0619])

5.3. Grand Canonical Monte Carlo method

Grand Canonical Monte Carlo (GCMC) method is statistical-stochastic, since it is based on the generation of random configurations.

The GCMC method is based on the Metropolis algorithm, which generates random configurations following a Markovian chain [33]. This algorithm is based on the fact that probability of an occurring event depends on the immediately previous event [33, 34].

By having a system in which all intermolecular interactions have been specified, then the Markov sequence has to be configured. In this step, it must be stipulated how to generate random test movements, which are the translation, rotation, insertion and deletion movements. So, in each step the movement executed is chosen at random. Depending to the new configuration of the system, the movement will be accepted or not [33]. Therefore, a rule is defined to accept or reject the molecule movement in the system. This is given by the difference between potential energy proceeded from the new movement and potential energy of the previous step: if this difference is negative the movement is accepted and if it is positive it can be rejected or accepted according to whether the number is greater or less than the expression $\exp(v(r_{ij})/kT)$ [33].

In a translation attempt, the new configuration is obtained as [33]:

$$\begin{aligned} x'^{N}{}_{i} &= x^{N}{}_{i} + \Delta(Rand - 0.5) \\ y'^{N}{}_{i} &= y^{N}{}_{i} + \Delta(Rand - 0.5) \\ z'^{N}{}_{i} &= z^{N}{}_{i} + \Delta(Rand - 0.5) \end{aligned} \tag{13}$$

Where the term *Rand* are random numbers between 0 and 1 and the term Δ is the maximum displacement, chosen to obtain a suitable fraction of accepted movements. Thus, if it is very small, most movements are accepted, but this leads to an inefficient sampling of the phase space. On the other hand, if it is very large, most movements are rejected. Hence, its adequate value depends on the interaction potential [33].

For rotational attempts, random rotations are generated as [33]:

$$r' = \begin{pmatrix} cos(\Delta\theta) & -sin(\Delta\theta) & 0 \\ sin(\Delta\theta) & cos(\Delta\theta) & 0 \\ 0 & 0 & 1 \end{pmatrix} \cdot r \qquad (14)$$

The scheme followed for the construction of a random route according to Metropolis is [38]:

1. A random particle is selected and its energy $U(r^N)$ is calculated.

2. This particle is randomly moved $r'^N = r^N + \Delta r$ and its new energy $U(r'^N)$ is calculated.

3. r'^N movement is accepted if:

$$acc(o \to n) = min(1, exp\{-\beta[U(n) - U(o)]\})$$

This means that it is based on minimization of energy and acceptance or rejection procedure is described below:

- ΔU < 0 → the movement is accepted, and it goes back to step 1.
- ΔU > 0 → a random number ζ is chosen between 0 and 1. Then:
  - ζ < exp(βΔU) → the movement is accepted, and it goes back to step 1.
  - ζ > exp(βΔU) →the movement is not accepted, consequently initial position of the particle is maintained, and it goes back to step 1.

4. This process is carried out with all the particles and after many steps, equilibrium is reached.

5. Other properties of interest are calculated from these results.

6. SIMULATIONS DETAILS

In the present simulations, the Ni-MOF-74 behaves consists on a rigid structure with atoms fixed in their positions. The FF parameters for the MOF structure are obtained from Bekker et al. [40]. In the case of CO_2, H_2, CH_4 and N_2 gas molecules, the FF parameters are taken from TraPPE-UA [41], and finally the parameters for SO_2 are obtained from Ketko et al. [42]. All these parameters corresponds to interactions between like atoms and are shown in Table 2.

Table 2. Lennard-Jones adsorbates parameters and charges.

MOLECULE	ATOM	σ [A]	ε/k_b [K]	q [e]
MOF	Ni	2.52	7.45	1.298
	C1	3.43	45.8	0.895
	C2			-0.349
	C3			0.418
	C4			-0.173
	O1	3.12	27.93	-0.789
	O2			-0.696
	O3			-0.785
	H	2.57	21.3	0.181
CO_2	C	2.8	27	0.7
	O	3.05	79	-0.35
N_2 (N-X-N)	N	2.958	36.4	-0.482
	X	--	--	0.964
H_2 (H-X-H)	H	3.02	27	0
	X	--	--	0
CH_4	C	3.73	148	0
SO_2	S	3.620	145.9	0.471
	O	3.010	57.4	-0.235

(a) X is the mass centre of these molecules (imaginary atom). It is considered that they have a centre of mass between their two atoms because they have a double link and it is a way to define their behaviour.

From these parameters and using Lorentz-Berhelot rules, parameters values for the interaction between different atoms are calculated.

All GCMC simulations have been performed by means of the LAMMPS package. [16, 17]. Each simulation consists of two million of GCMC steps, where the first half of steps corresponds to the equilibrium stage, and the second half to the production stage, from which all averages are computed. In Figure A1 (Appendix), an example of simulation is reproduced.

Table 3 shows the values used to calculate the energetic costs.

Table 3. Ni-MOF-74 properties.

Density	**ρ [kg/m³]**	1185
Heat capacity	**C_p [kJ/kg·K]**	0.9
Bed voidage	**ϵ**	0.4
Bed volume	**V [m³]**	1

In Swing Adsorption Processes, two beds are simulated at constant temperature/pressure in parallel, in which while one bed adsorbs, the other desorbs. This is called Skarstrom's four-step cycle (2+2) [43], which was adapted by Chung et al. [44]: pressurization (I) and adsorption (II) correspond to the adsorption phase, and, on the other hand, depressurization/purge (III) and evacuation (IV) are grouped in desorption.

The adiabatic work for compression (PSA) or expansion (VSA) during one adsorption cycle can be calculated with the equation proposed by Chaffee et al. [45] and Riboldi et al. [46] This equation, in case of PSA, is [16]:

$$W_{PSA} = \left(\frac{k}{k-1}\right)\frac{R\cdot T}{\eta}\left[\frac{P_{ads}\cdot V\cdot \epsilon}{R\cdot T} + \frac{WC_{CO_2}}{y_{CO_2}}\cdot m\right]\left(\left(\frac{P_{ads}}{P_{des}}\right)^{\frac{k-1}{k}} - 1\right) \qquad (15)$$

Where *m* is Ni-MOF-74 mass, WC_{CO2} is the working capacity of CO_2 under conditions studied and y_{CO2} is CO2 partial pressure at feed, P_{ads} is the adsorption pressure, P_{des} is the atmospheric pressure and polyentropic coefficient *k* is considered 1.4 (air).

In case of VSA, the expression is [16]:

$$W_{VSA} = \left(\frac{k}{k-1}\right)\frac{R \cdot T}{\eta}\left[\frac{P_{ads} \cdot V \cdot \epsilon}{R \cdot T} + N_{TOT}^{ads} \cdot m\right]\left(\left(\frac{P_{ads}}{P_{des}}\right)^{\frac{k-1}{k}} - 1\right) \quad (16)$$

Where $N^{ads}{}_{TOT}$ is the sum of all adsorbed amount of mixture components. This is assumed because there is no purge step to completely regenerate bed. On the other hand, m is Ni-MOF-74 mass, P_{ads} is the atmospheric pressure and P_{des} is the desorption pressure. In VSA, polyentropic coefficient k is 1.28 (CO_2), since it is assumed that practically everything is CO_2. In the two previous cases, the first term corresponds to gas present in the empty volume of the bed and the second term to gas that is in the MOF. On the other hand, the thermal regeneration energy in TSA can be calculated as [17]:

$$\mathcal{Q} = \frac{P \cdot V \cdot \epsilon}{R \cdot T} \cdot \frac{7}{2} \cdot R \cdot \Delta T + m \cdot (C_p \Delta T + \sum q_{st} \cdot \Delta q) \quad (17)$$

Where m is the Ni-MOF-74 mass, Cp is the heat capacity and ΔT is the difference between desorption temperature and adsorption temperature. Adsorption temperature in this study is constant and its value is 313K, while desorption temperature varies between 383K and 473K. The first term refers to heating gas that is in the empty volume, the second term to heating the MOF structure (it also approximates heating of internal gas in the MOF) and the last term to break bonds between adsorbent and adsorbate.

Finally, the energy index is calculated, which is the energy needed in GJ to separate a ton of CO_2.

7. RESULTS AND DISCUSSION

7.1. Validation

The accuracy of the FF used in the present work has been checked by comparing the results obtained from GCMC simulations with available experimental data. Validation was previously done in a previous study [47], in which the amount of CO_2 adsorbed was plotted against the pressure at 298K. Figure A2 (Appendix) shows that results obtained are very similar to those obtained experimentally by Queen et al [48]. Therefore, we can rely on the results provided by this FF.

Figure 11 shows a snapshot of the Ni-MOF-74 structure interacting with a low-pressure CO_2 flue gas (in green), showing the high affinity of these molecules for the unsaturated metal atoms (blue). Hence, the first CO_2 adsorbed molecules occupy the sites close to the metal atoms. As pressure increases, more CO_2 molecules are adsorbed filling the empty space until the material is saturated.

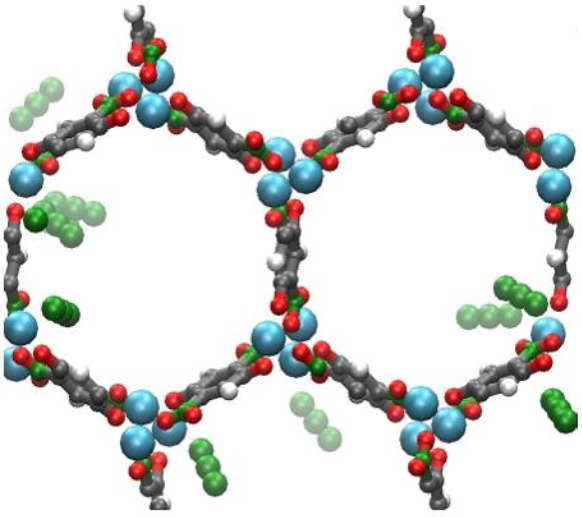

Figure 11. Preferential sites of CO_2 in Ni-MOF-74 at 0.01 atm. (taken from: [47])

7.2. Pure components

Adsorption isotherms and isobars for pure components allow us to know which molecules have more affinity for the material and therefore will present a higher uptake. The gases involved in the present work include carbon dioxide (CO_2), nitrogen (N_2), sulfur dioxide (SO_2), hydrogen (H_2) and methane (CH_4), as they are present in the industrial mixtures selected for this study: a) post-combustion gas mixture without impurities (CO_2/N_2) and b) with impurities ($CO_2/N_2/SO_2$); c) the synthesis gas mixture (CO_2/H_2), and d) biogas mixture (CO_2/CH_4).

All adsorption isotherms have been calculated at 313K, according to the typical temperature at which PSA and VSA cycles are performed. Similarly, all adsorption isobars have been computed at atmospheric pressure, which corresponds to the operating pressure in a TSA unit. For clarity, the x-axis (pressure) of the adsorption isotherms has been plotted using a logarithmic scale.

Figure 12 shows the pure-gas adsorption isotherms. The amount of adsorbed component, in moles of gas per kilogram of adsorbent (mass uptake), as a function of the pressure is shown in the range 0.01 to 10 bar.

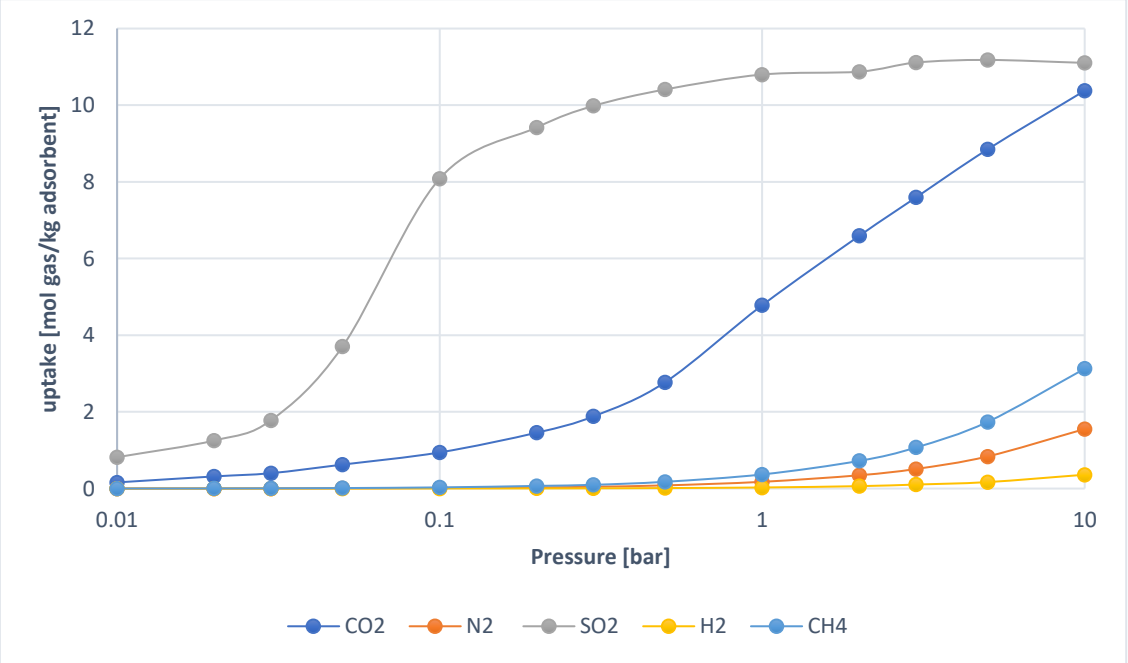

Figure 12. Pure components adsorption isotherms at 313K (lines are guides to the eyes).

As pressure increases, the amount of gas molecules adsorbed becomes higher. In addition, this figure shows that CO_2 has a high affinity for Ni-MOF-74, since its uptake is much higher than that of N_2. CH_4 and H_2 in all the pressure range. This result suggests a high selectivity for CO_2. However, the mass uptake of SO_2 is even greater, especially at low and intermediate pressures. This means that SO_2, which is an impurity in post-combustion mixtures, can greatly affect separation performance of Ni-MOF-74. Note that, at high pressures, the amount of SO_2 adsorbed becomes constant due to the fact that solid adsorbent becomes saturated (all the pores are occupied, and the material cannot adsorb any more molecules).

Similarly, the mass uptake as a function of the temperature (adsorption isobar) is shown in Figure 13, with the temperature ranging from 313K to 413K.

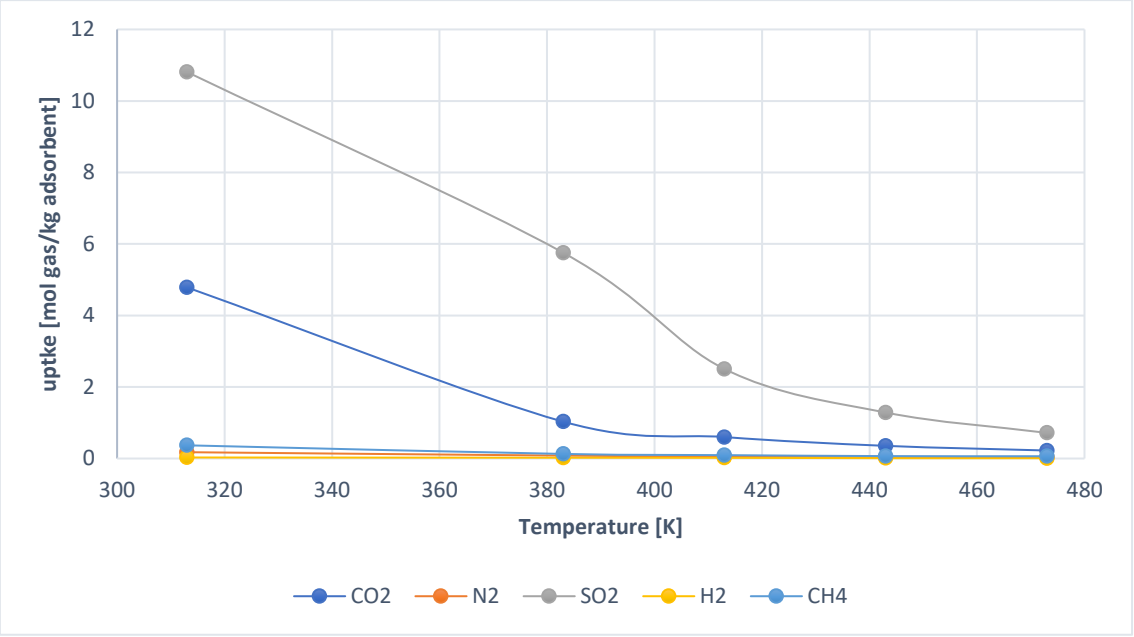

Figure 13. Adsorption isobars of pure components at atmospheric pressure (lines are guides to the eyes).

As temperature increases, the amount of adsorbed molecules decreases. As in the previous case, SO_2 presents the highest uptakes in all the temperature range studied, followed by CO_2, CH_4, N_2 and H_2.

The isosteric heat (q_{st}) for each adsorbed molecule can be calculated from GCMC simulations of pure-gas components. As stated in the previous chapter, this property determines the energy required to desorb a molecule. Hence, a greater affinity with the material implies a much expensive desorption (higher isosteric heat).

Table 4 shows the values of the isosteric heat for the different components obtained from GCMC simulations:

Table 4. Isosteric heats of components selected.

MOLECULE	Isosteric heat [kJ/mol]
CO_2	34.3
N_2	10.7
SO_2	37.2
H_2	7.6
CH_4	13.8

As expected, SO_2 has the highest value, followed by CO_2, CH_4, N_2 and H_2.

7.3. Post-combustion mixture

According to the typical post-combustion gas composition, the following binary mixture has been considered in our simulations: CO_2 (15%), and N_2 (85%). Again, GCMC simulations have been carried out to obtain the adsorption isotherms and isobars for the binary mixture. As for pure-components, a pressure range between 0.01 to 10 bar and a temperature range between 313 to 473K has been considered for the adsorption isotherms and isobars, respectively This data will allow us to calculate all the adsorbent evaluation criteria.

A comparison between the uptake of pure-gas CO_2 and N_2 and its uptake in the post-combustion mixture is shown in Appendix. As shown in Figure A3, the behaviour of both gases in the binary mixture is very similar to their behaviour as pure-gases, except for N_2 at high pressures, where its uptake in the binary mixture is lower than expected.

Again, the amount of CO_2 adsorbed is much greater than that of N_2, which remains practically constant.

The effect of SO_2 impurities in the CO_2 separation performance of Ni-MOF has been studied for SO_2 compositions of 0.01%, 0.1%, and 1%, which are compared with the results for the post-combustion mixture without impurity. In all these cases, the CO_2 composition in the ternary mixture is 15%, and the nitrogen percentage ranges from 84 to 84.99%.

The CO_2 uptake as function of pressure for different concentrations of SO_2 is plotted in Figure 14, showing very small differences for all mixture compositions.

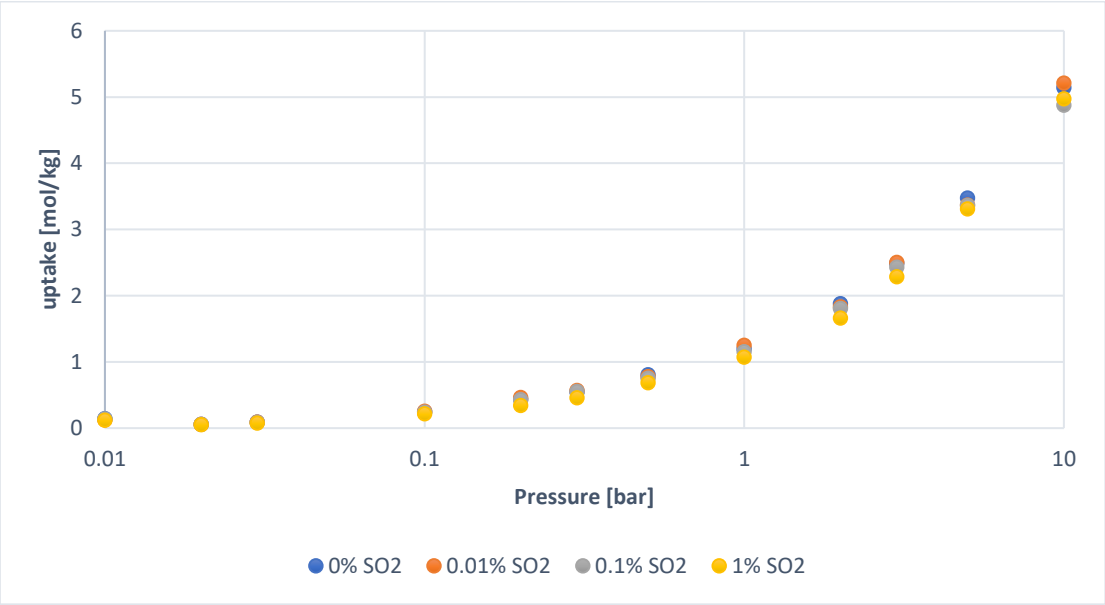

Figure 14. Uptake comparation of post-combustion gases with SO_2 impurities.

The effect of SO_2 impurities on the selectivity of CO_2 over the other components (N_2 and SO_2) has been also studied, as shown in Figure 15. As expected, the highest selectivity of CO_2 is given by a mixture without impurities, while the lowest selectivity is obtained for the ternary mixture with a SO_2 composition of 1%. This fact is a consequence of the competition between SO_2 and CO_2 molecules for the available adsorption sites.

It can also be observed that, for a SO_2 composition of 1%, the selectivity of CO_2 is very low and remains practically constant through all pressure range, since the uptake of SO_2 is very high even at low pressures. For a SO_2 composition of 0.1%, the selectivity also remains constant, although its value is higher. Finally, the CO_2 selectivity for 0% and 0.01% of SO_2 decreases as the pressure is increased, since more SO_2 is adsorbed. Overall,

the selectivity values obtained for mixtures with an impurity concentration of 0.1% or lower are really high.

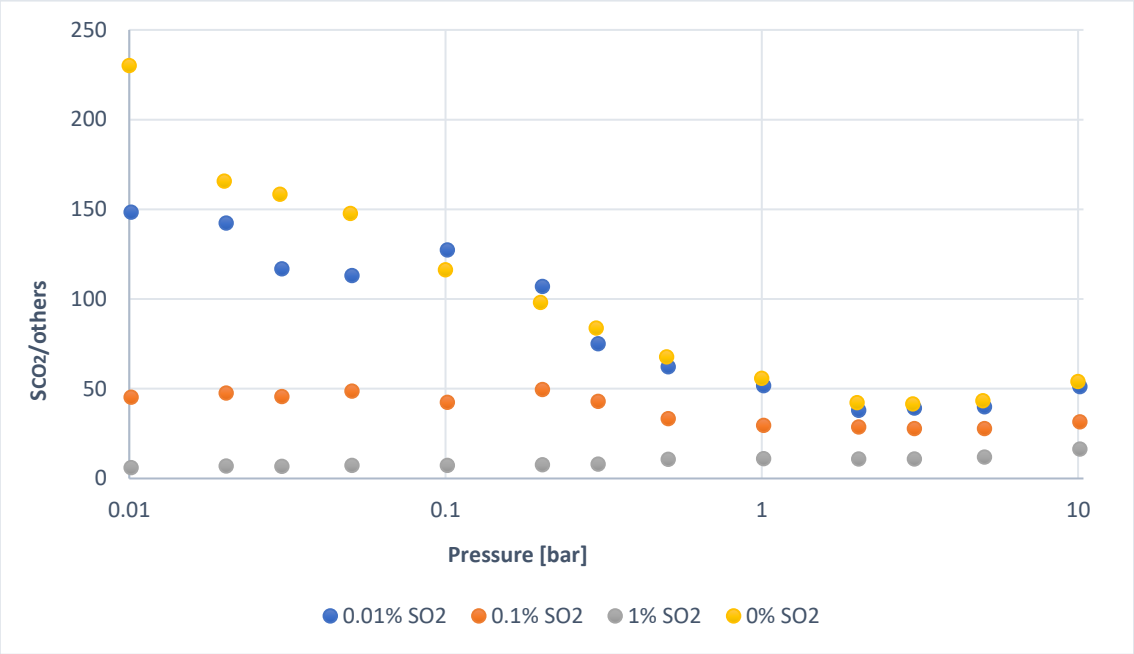

Figure 15. CO_2 selectivity over other components.

Another important parameter to study is the CO_2 working capacity, which has been explained in Section 4.4.4.

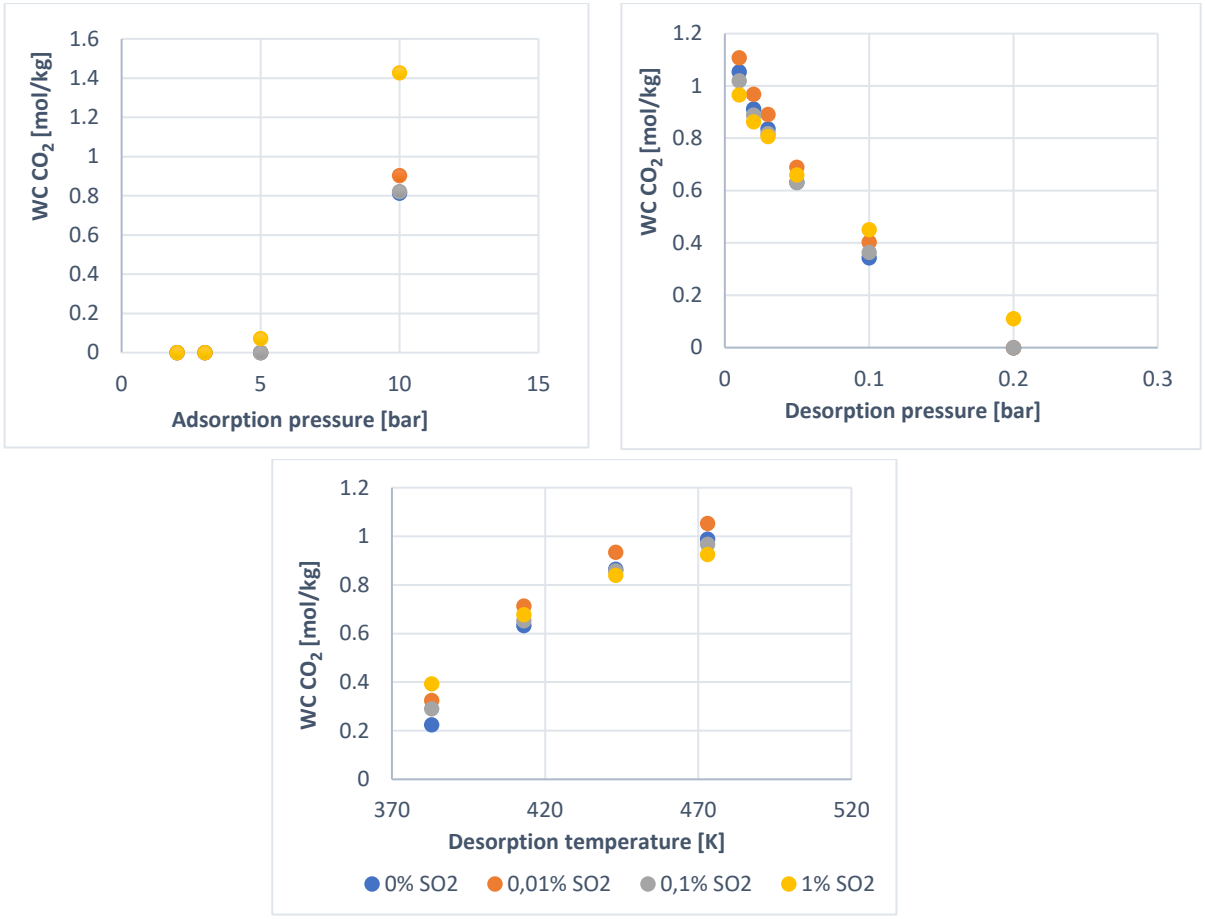

Figure 16. CO_2 working capacities in PSA (Tdes=1 bar), VSA (Tads=1 bar) and TSA (Tads=313K)..

The working capacity of CO_2 as function of the adsorption pressure in a PSA unit is shown in Figure 16. As expected, the working capacity increases as the adsorption pressure becomes higher, since the desorption pressure is always the atmospheric pressure. Surprisingly, the working capacity for CO_2 is greater when SO_2 is added as an impurity. This could be a consequence of the appearance of attractive lateral interactions between CO_2 and SO_2 molecules at high pressures, resulting in an increase of the working capacity for both components. Note also that, in order to be able to capture CO_2, the adsorption pressure must be at least 5 bar. For lower values, the pressure difference between adsorption and desorption steps is not enough and the working capacity is zero.

Figure 16 also shows the working capacity of CO_2 as function of the desorption pressure in a VSA unit. Again, the amount of CO_2 captured at each cycle is greater as the

desorption pressure is lowered. Interestingly, the presence of SO_2 impurities in the post-combustion mixture may either slightly increase or decrease the working capacity, depending on the operating conditions.

Finally, the working capacity of CO_2 as function of the desorption (or regeneration) temperature in a TSA unit is also shown in Figure 16. As expected, the working capacity increases as we increase the regeneration temperature, due to the higher amount of adsorbate molecules that desorb at high temperature. The presence of SO_2 also have an impact on the working capacity, especially when operating with a desorption temperature of 383K. However, there is no clear trend on whether higher composition of impurity will raise or lower the working capacity.

Next, the purity of the CO_2 captured at outlet of the bed in the different swing adsorption processes is studied. This parameter is very important if the separated CO_2 is expected to be used for other applications. Figure 17 shows the CO_2 purity at outlet in PSA, VSA and TSA.

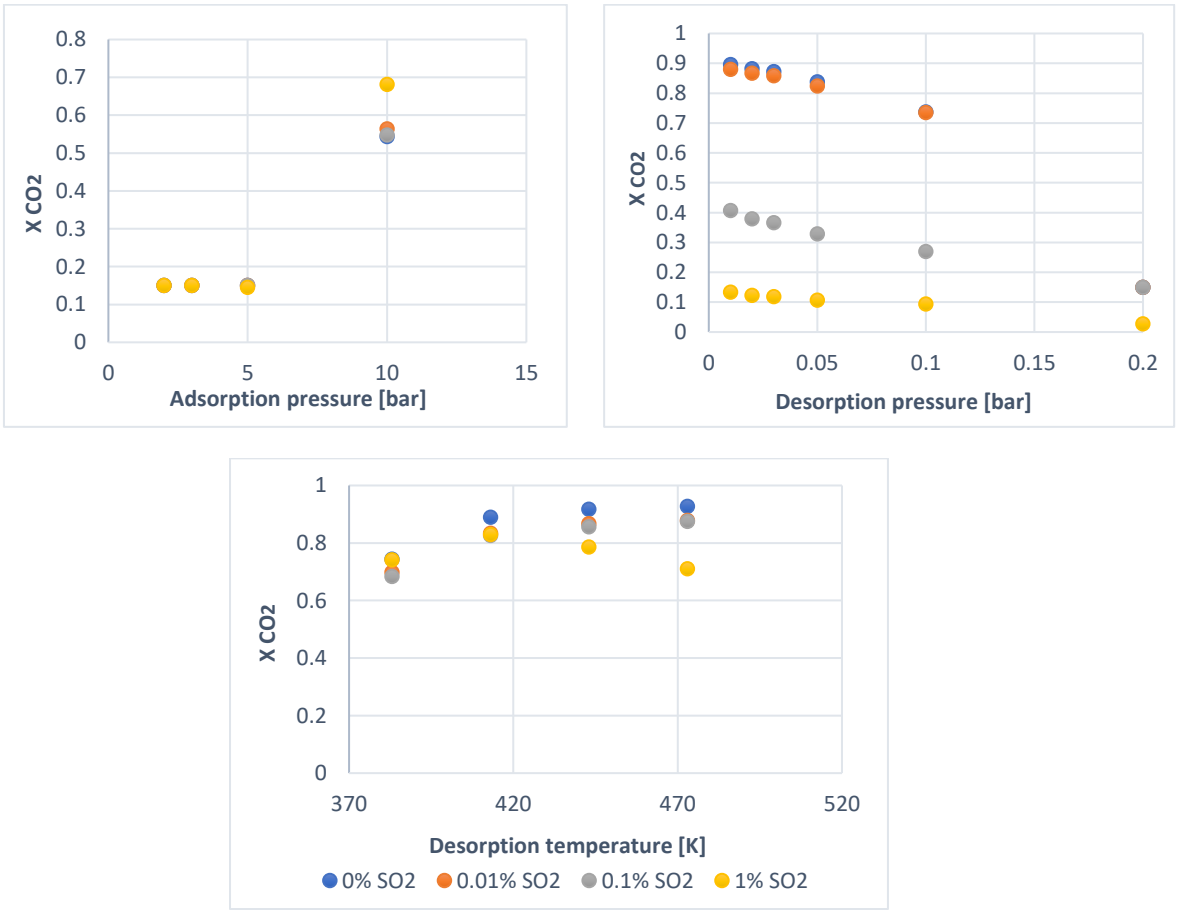

Figure 17. CO_2 purity in PSA, VSA and TSA.

Purity in PSA unit is a function of the adsorption pressure. At adsorption pressures of 5 bar or lower, the purity of CO_2 is only 15%, the same than in the post-combustion mixture, since at these conditions Ni-MOF-74 is not effective for CO_2 capture. However, if the adsorption pressure is raised to 10 bar, a purity around 55-70% can be achieved. Surprisingly, the highest purity value is obtained when the composition of the impurity is maximum (1%).

The purity at outlet as function of the desorption pressure in VSA is also shown in Figure 17. Interestingly, high purity values up to 90% can be achieved for low desorption pressures and when the concentration of SO_2 is lower than 0.01%. However, larger amounts of the impurity cause a detrimental impact in the final purity. At a desorption pressure of 0.01 bar, for instance, the purity decreases from 90% to 41% when the amount of SO_2 in the post-combustion mixture is 0.1%, or to only 13% when its concentration is 1%.

Finally, the CO_2 purity at outlet of the bed in a TSA unit as function of the desorption temperature is reproduced. Interestingly, the purity is quite high in all operating conditions, and increases as the desorption temperature is raised, surpassing 90% at desorption temperatures of 443K or higher. The presence of SO_2 have a negative impact on the final purity, especially at high desorption temperatures, since the adsorbed SO_2 is also released.

In order to analyse the energy requirements, the adiabatic work for compression or expansion in PSA and VSA, respectively, as well as the thermal regeneration energy in TSA have been calculated (see Section 6). The energy index is defined as the energy (in GJ) needed to separate a ton of CO_2. In Figure 18, the energy index and the working capacity obtained for the different Swing Adsorption under a range of operating conditions is plotted.

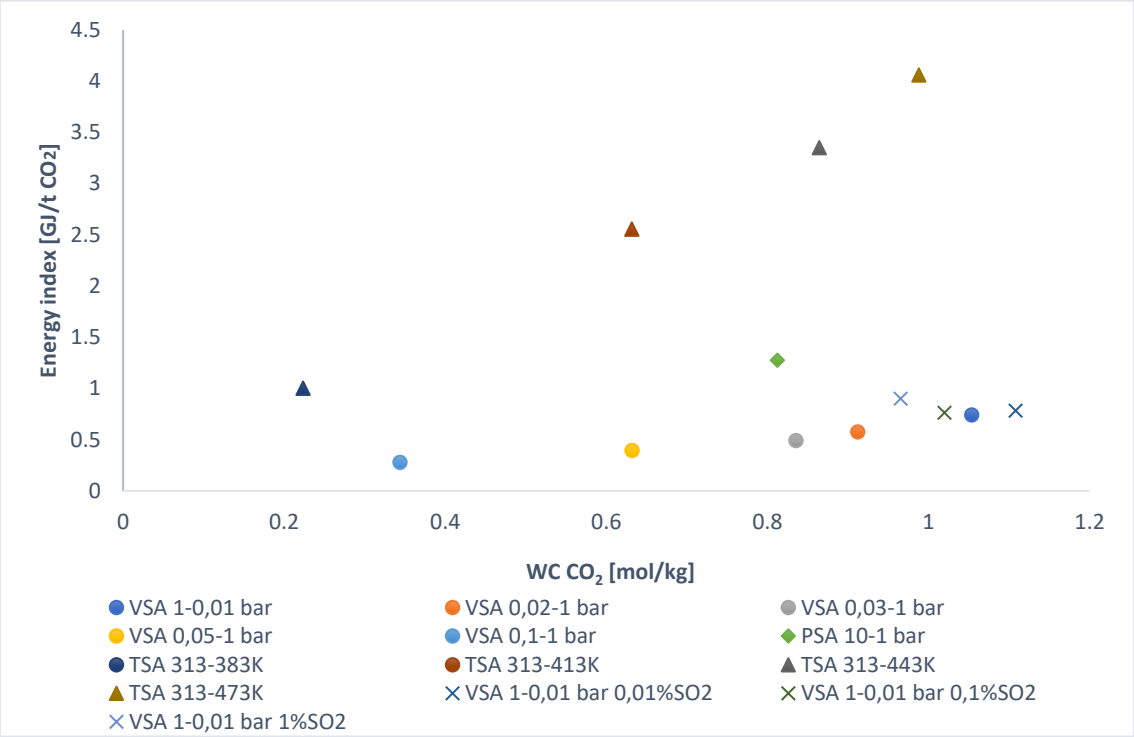

Figure 18. Energy index in PSA, VSA and TSA.

The ideal process is the one presenting a very high working capacity per cycle (since this will decrease the frequency at which the solid adsorbent must be regenerated) and also a low energy index. The most energetically attractive process to capture CO_2 from post-combustion mixtures is VSA with a desorption pressure of 0.01 bar, since it presents the highest working capacity and a low energy index. Moreover, a purity value of 90% can be achieved. After selection this process as the best candidate, we have studied how the presence of SO_2 affects its performance (see the crosses in Figure 18). It is shown that the presence of SO_2 in large quantities (0.1 and 1%) decreases working capacity of CO_2 and slightly increases energy index. However, with a SO_2 concentration of 0.01%, the energy index also increases slightly but the working capacity is even higher. Hence, the presence of a concentration of 0.01% SO_2 is not detrimental to this process. If the concentration is 0.1 or 1%, this process will still present suitable values of energy index and working capacity, but the purity at outlet will be much lower (see Figure 17).

7.4. Biogas

Biogas is a binary mixture composed of carbon dioxide and methane. Two typical compositions are 1) 40% of CO_2 and 60% of CH_4, and 2) 50 of CO_2 and 50% of CH_4 [49]. Both of them have been analysed in the present work.

A comparison between the uptake of pure-gas CO_2 and CH_4 and its uptake in the biogas mixture is shown in Appendix. As shown in Figure A4, the behaviour of both gases in the binary mixture is very similar to their behaviour as pure-gases, except for CH_4 at high pressures, where its uptake in the binary mixture is lower than expected. The amount of CO_2 adsorbed is much greater than that of N_2, which remains practically constant. The amount of CO_2 adsorbed is higher than the amount of CH_4 in all the pressure range studied.

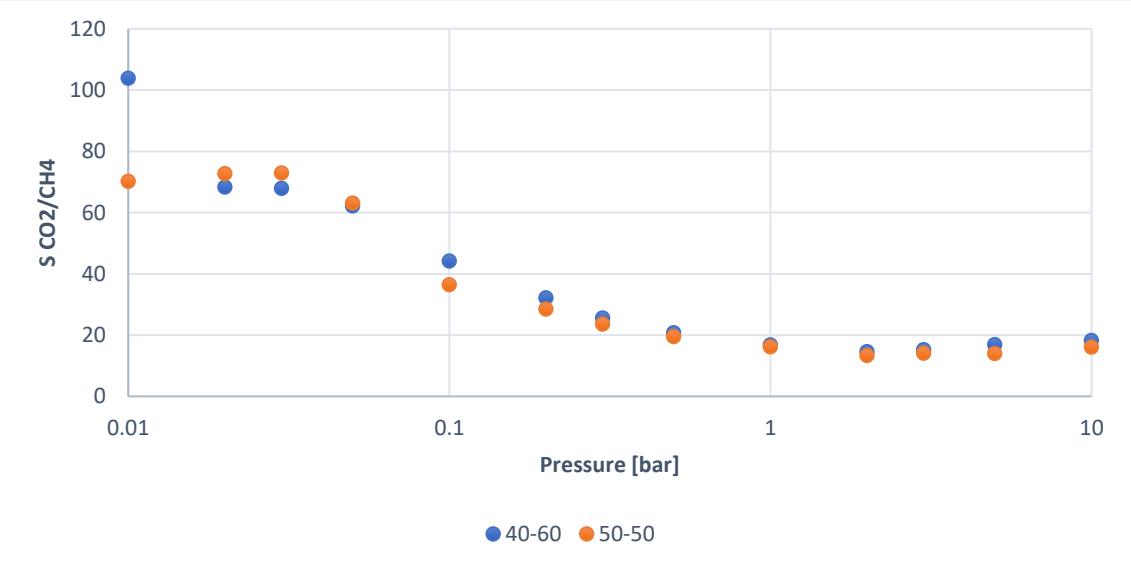

Figure 19. CO2 selectivity (T=313K).

The selectivity of CO_2 over methane in Ni-MOF-74 has been plotted in Figure 19. Both compositions present very similar selectivity values, and the highest values are achieved at low pressures. In general, the selectivity of CO_2 over methane in biogas mixtures is lower than the selectivity of CO_2 over nitrogen in post-combustion mixtures.

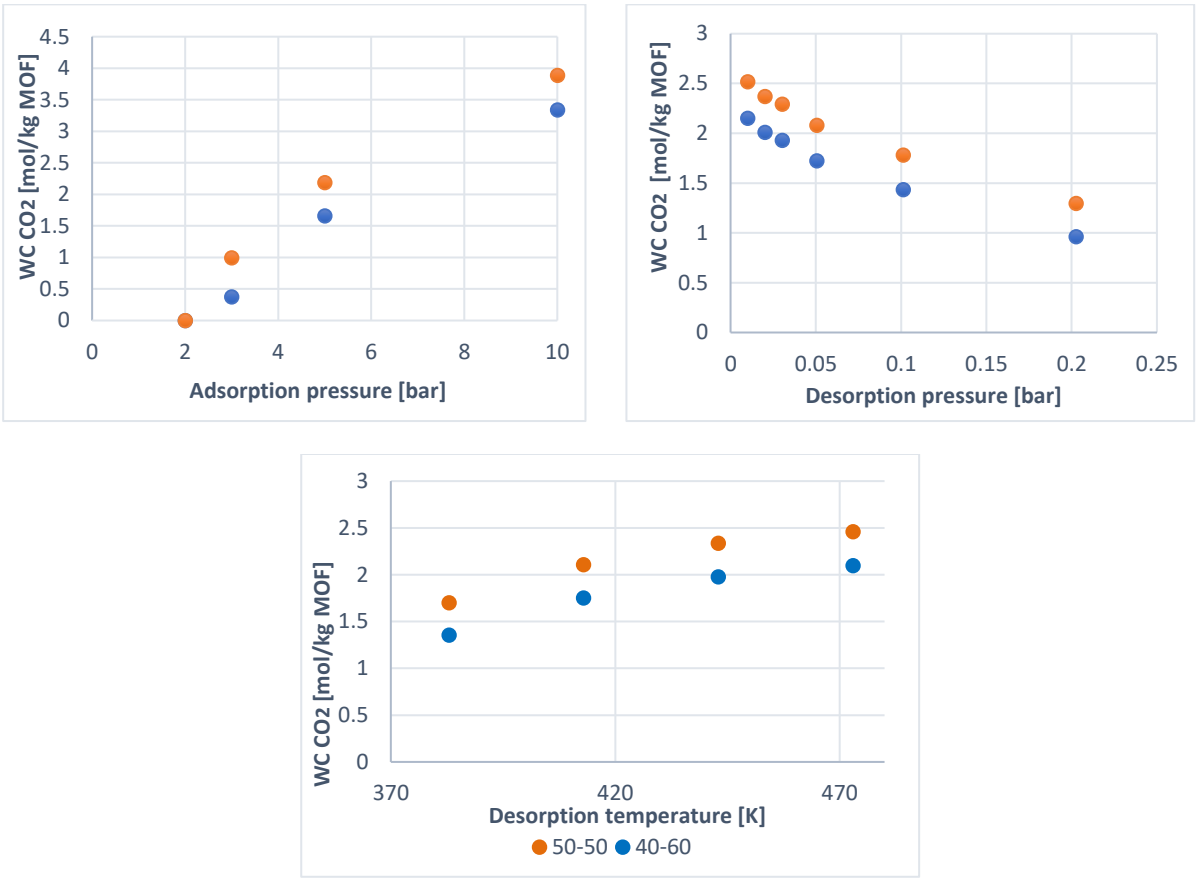

Figure 20. Working capacity of CO_2 in PSA, VSA and TSA.

The working capacity of CO_2 as function of the adsorption pressure in a PSA unit is shown in Figure 20. In contrast to the results obtained for the post-combustion mixture, it is possible to capture non-negligible values of CO_2 from adsorption pressures of 3 bar. Moreover, the working capacity for biogas is much greater than that of a post-combustion mixture, with values up to 4 moles of CO_2 per kilogram of adsorbent at an adsorption pressure of 10 bar. This is a result of the higher composition in CO_2 on the former (40-50%) compared to the latter (15%). For that reason, a 50:50 mixture presents higher working capacities than 40:60.

The working capacity of CO_2 as function of the desorption pressure in a VSA unit is also shown in Figure 20. Again, the biogas mixture presents much higher working capacity values than the post-combustion mixture, being the 50:50 mixture the one providing the highest values in all the pressure range studied. The increase of the working capacity as

the desorption pressure is lowered is still observed, but it is less sharp compared to the results obtained for the post-combustion mixture (see Figure 16).

Finally, the working capacity of CO_2 as function of the desorption temperature in a TSA unit is plotted. Again, the values are much higher than for the post-combustion mixture. For instance, the working capacity for a 50:50 biogas mixture at the lowest desorption temperature (383K) is around 1.7 mol·kg^{-1}, while that of the post-combustion mixture at the highest desorption temperature (484K) is only 1 mol·kg^{-1}.

The purity of CO_2 at outlet of the adsorber for the three Swing Adsorption Processes as function of the operating conditions is plotted in Figure 21.

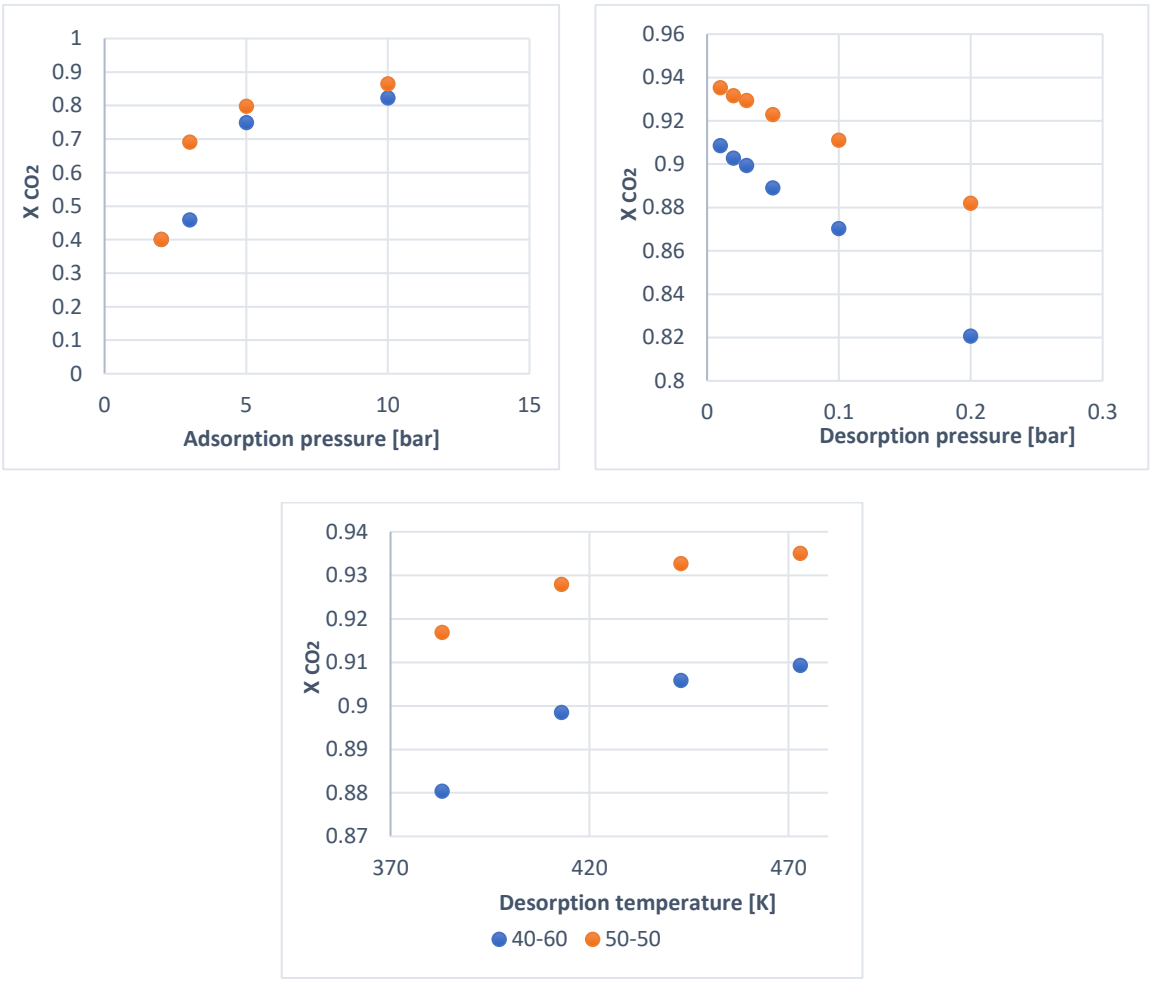

Figure 21. CO_2 purity in PSA, VSA and TSA.

Results show that the purity raises as the difference between the adsorption and desorption pressure (in PSA and VSA) or temperature (in TSA) increases. The highest purity values are obtained for VSA or TSA, as for the post-combustion mixture, with values up to 94%, which is very suitable for further utilization of the CO_2. As expected, the 50:50 mixture presents higher purity values than the 40:60 mixture.

The energy index for the three swing adsorption processes have been calculated for both biogas mixtures (see Figures 22 and 23). A competitive energy index should be lower than 1 GJ per ton of CO_2 captured. Hence, the most suitable process corresponds to a VSA unit operating at 1-0.03 bar for the 40:60 mixture, and a PSA unit operating under 5-1 bar for the 50:50 mixture.

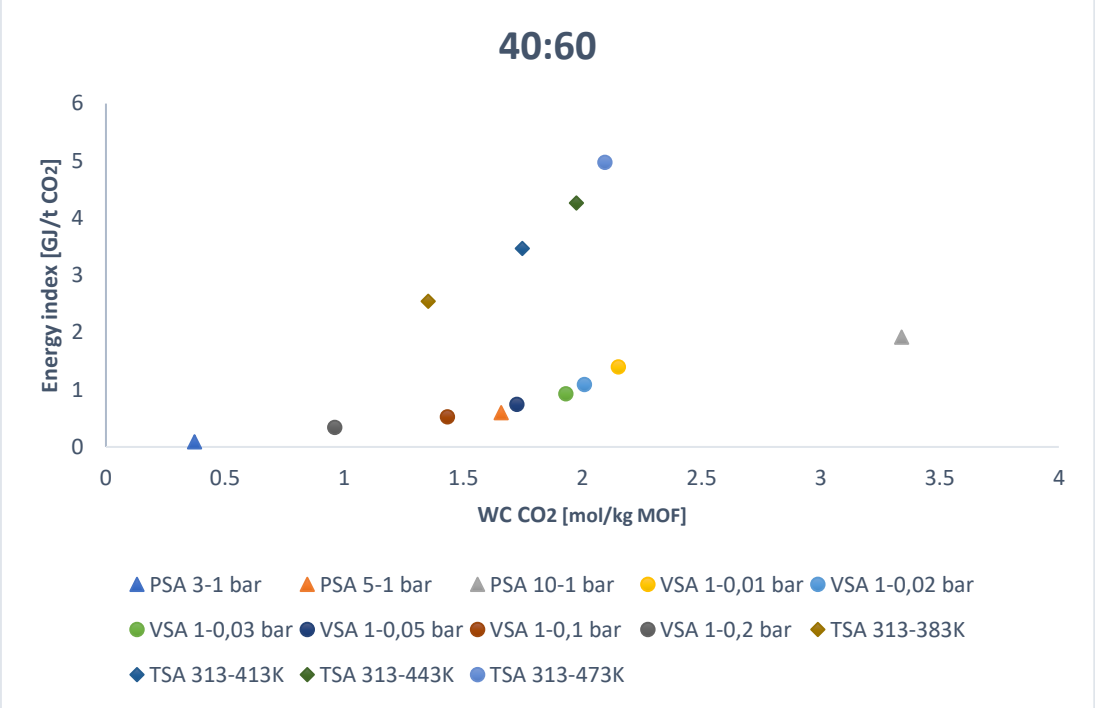

Figure 22. Energy index of 40:60 composition of biogas.

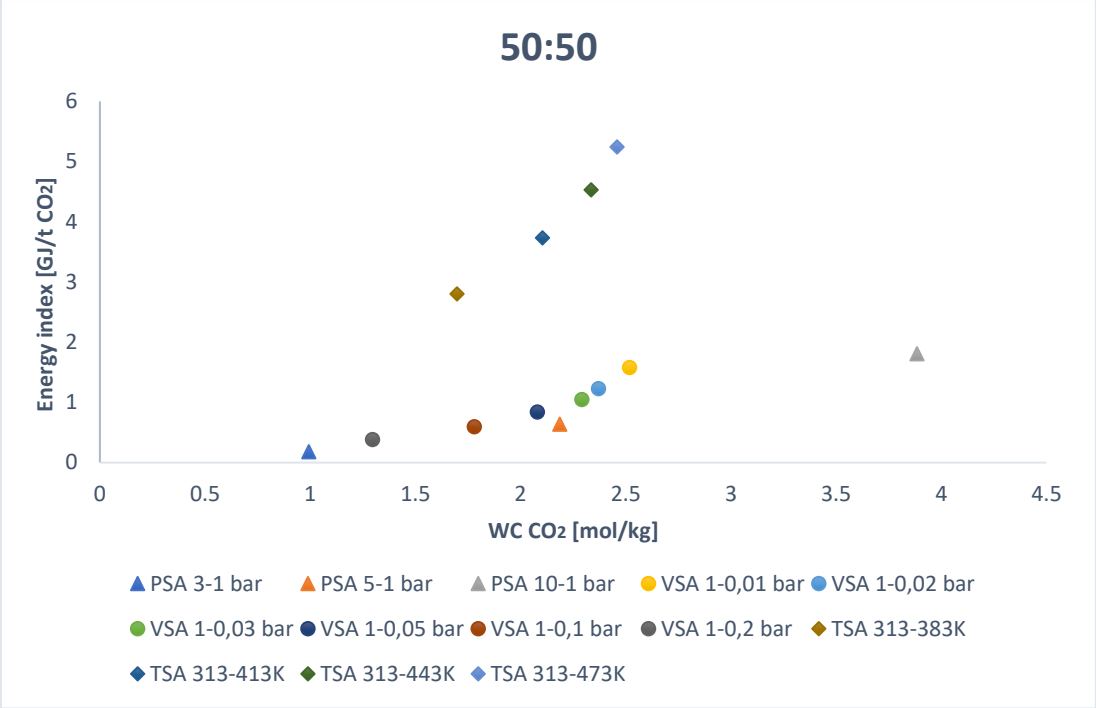

Figure 23. Energy index of 50:50 composition of biogas.

7.5. Syngas

Syngas is a binary mixture composed by 30% of CO_2 and 70% of H_2. It is one of the typical gas streams which contains CO_2 and has to be separated. A comparison between the uptake of pure-gas CO_2 and H_2 and its uptake in the syngas mixture is shown in Appendix. As shown in Figure A5, the behaviour of both gases in the binary mixture is very similar to their behaviour as pure-gases in all pressure range.

The selectivity of CO_2 over hydrogen in Ni-MOF-74 has been plotted in Figure 24. Surprisingly, the selectivity of CO_2 over hydrogen is incredibly high, much more than that of CO_2 over nitrogen or CO_2 over methane in post-combustion and biogas mixtures, respectively, reaching values up to 2000 at low pressure.

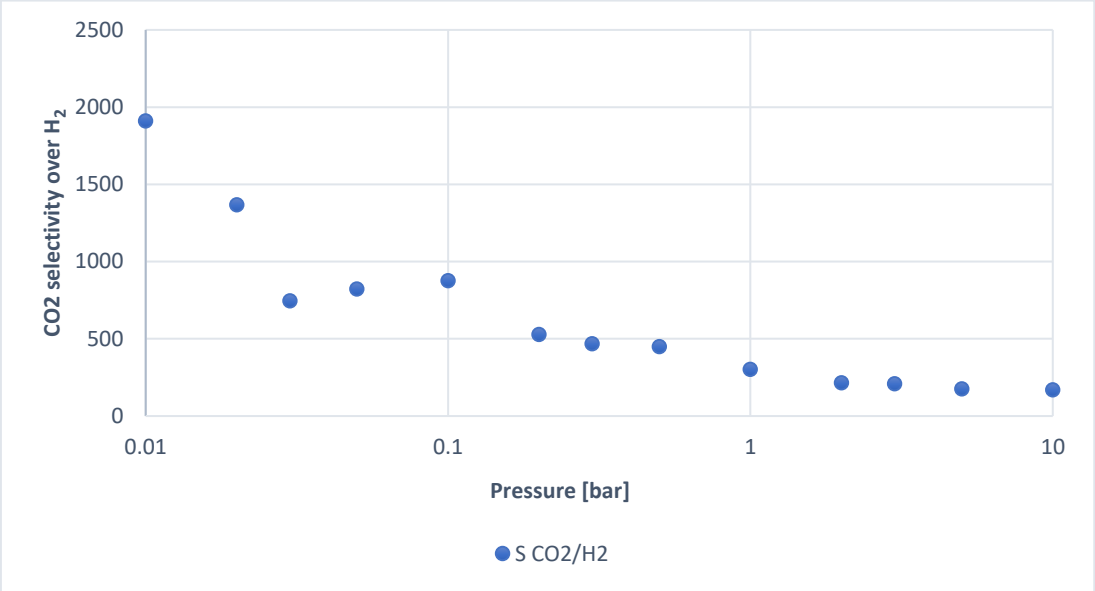

Figure 24. CO2 selectivity over H2 in syngas mixture.

The working capacity values of CO_2 as function of the adsorption pressure in PSA, the desorption pressure in VSA and the desorption temperature in TSA are shown in Figure 25. The values obtained are higher than in the post-combustion mixture, where the CO_2 composition is 15%, but lower than in the biogas mixture, which contains between 40-50% of CO_2. The maximum working capacity is achieved for a PSA unit operating under 10-1 bar.

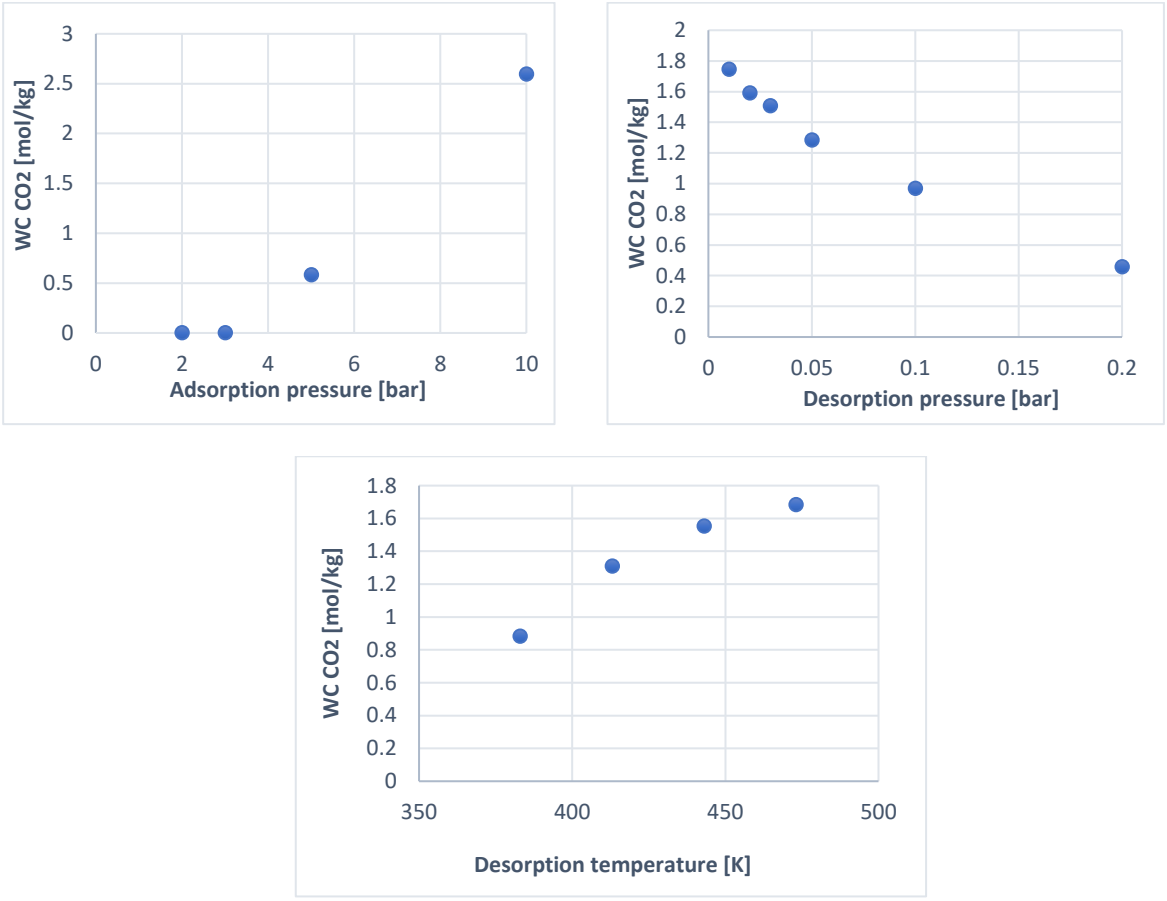

Figure 25. Working capacity of CO_2 in PSA, VSA and TSA.

The purity of CO_2 at outlet of the adsorber for the three Swing Adsorption Processes as function of the reaction conditions is plotted in Figure 26. As in the previous mixtures, the purity raises as the difference between the adsorption and desorption pressure (in PSA and VSA) or temperature (in TSA) increases. The highest purity values are obtained for VSA or TSA, with extremely high values up to almost 99%, which is great for further utilization of the CO_2. This is due to the also extremely high selectivity of Ni-MOF-74 for CO_2 over hydrogen.

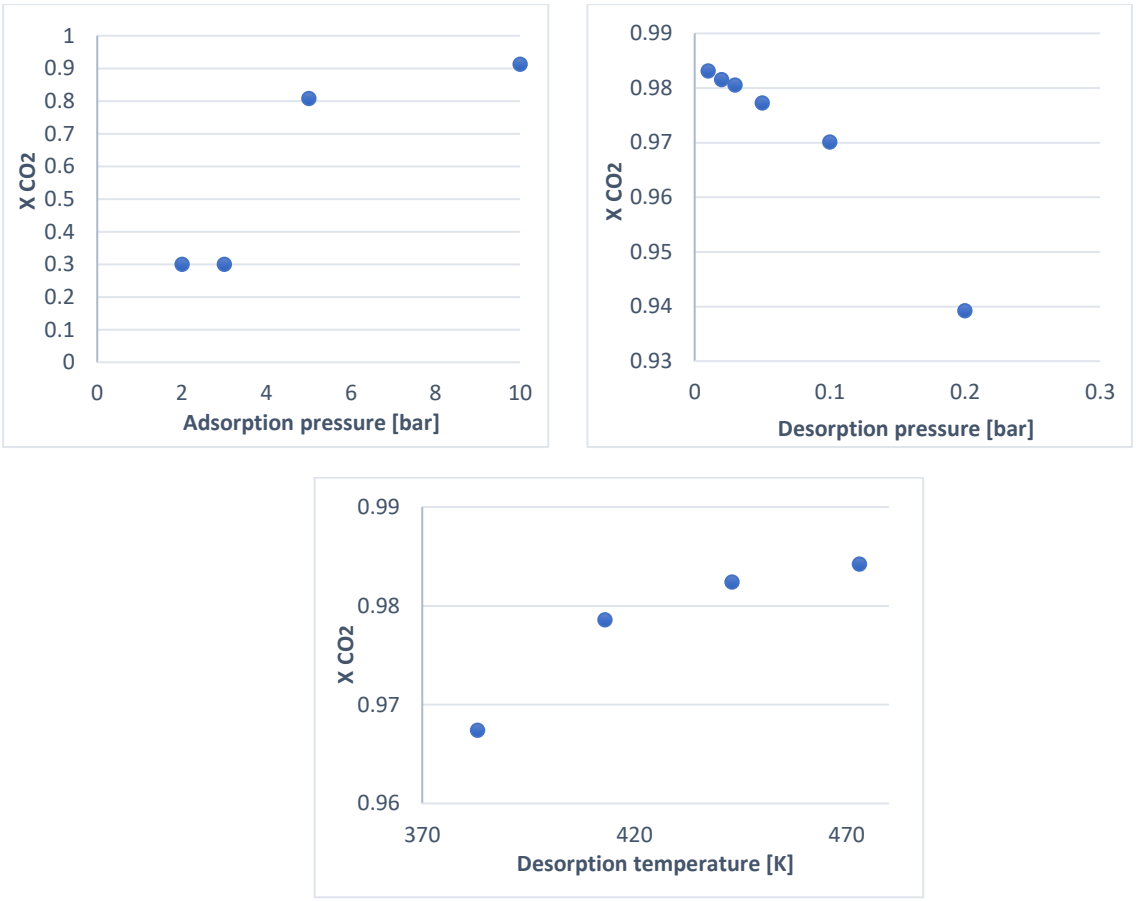

Figure 26. CO_2 purity in PSA, VSA and TSA.

The energy index for the three Swing Adsorption Processes have been calculated for the syngas mixture (see Figure 27). A competitive energy index should be lower than 1 GJ per ton of CO_2 captured. Hence, the most suitable process corresponds to a VSA unit operating with a desorption pressure between 0.02 and 0.03 bar.

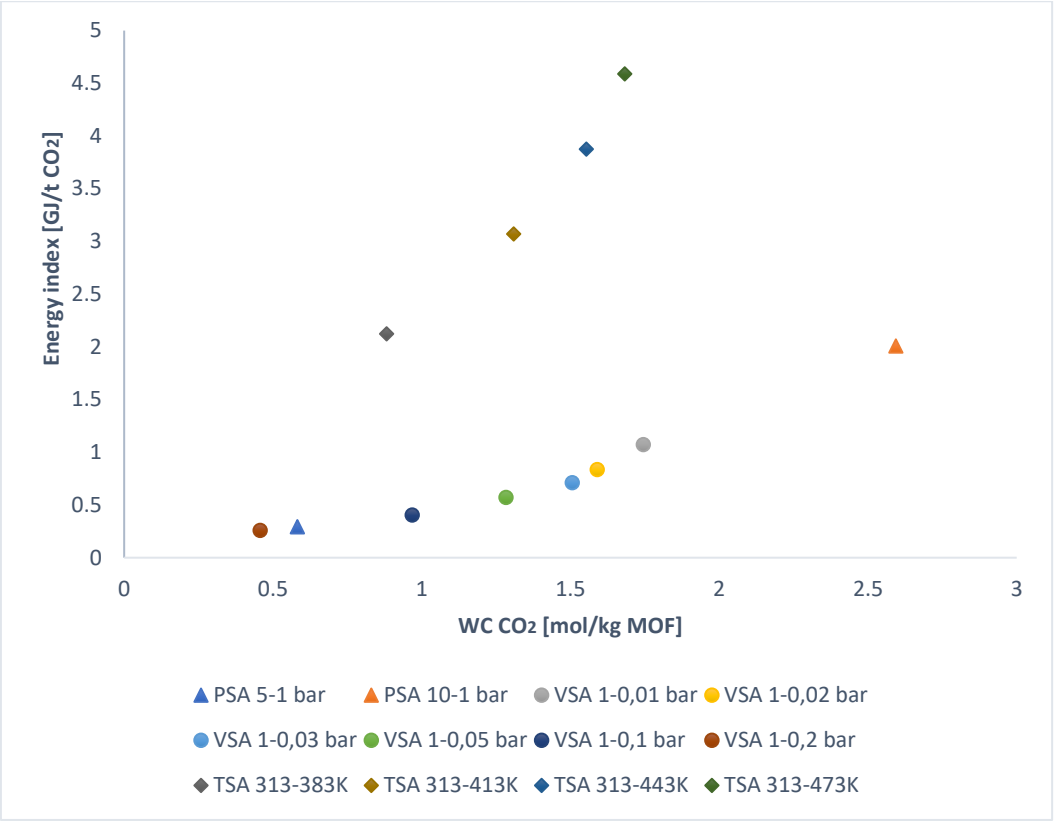

Figure 27. Energy index of syngas.

8. CONCLUSIONS

The aim of this chapter is to present all the conclusions of the master thesis in an ordered an summarized manner, in order to provide with a general view of the work:

- Ni-MOF-74 has a high affinity with carbon dioxide and weak interactions with the other main components of the mixtures, such as N_2, CH_4 and H_2. Therefore, the selectivity of the MOF towards CO_2 over other components is quite high.
- To select the most suitable Swing Adsorption Process, a compromise must be reached between low energy index and high working capacity. The most suitable process for the separation of CO_2 from a post-combustion mixture is VSA with desorption pressure of 0.01 bar, since it is the one that responds to a higher working capacity and an energy index of less than 1 GJ per ton of CO_2. In case of biogas, the most suitable process corresponds to a VSA unit operating at 1-0.03 bar for the 40:60 mixture, and a PSA unit operating under 5-1 bar for the 50:50 mixture. Finally, the most suitable process for a syngas mixture is VSA with desorption pressures between 0.02 bar and 0.03 bar, although there are many processes with an acceptable working capacity and very low energy index, such as VSA 1-0.2 bar or PSA 5-1 bar.
- In all mixtures, the SAP with the highest energy index is the Temperature Swing Adsorption. Hence, it would not be a good option in any case due to the high energy requirements.
- The presence of SO_2 impurities with a concentration of 0.01% or lower in post-combustion mixture does not significantly affect the adsorption performance of Ni-MOF-74. However, if the composition is 0.1% or higher the energy index slightly increases and the CO_2 purity at the outlet of the bed is considerably lower.

9. NOTATION

ads	adsorption conditions
CCS	Carbon capture and separation
CCSU	Carbon capture, separation and utilization
Cp	Heat Capacity [J/mol K]
des	desorption conditions
E	Activation energy
FF	Force Field
GCMC	Grand Canonical Monte Carlo
k	Polytropic parameter of gases
LJ	Lennard-Jones
MC	Monte Ccarlo
MD	Molecular Dynamics
MOF	Metal Organic Framework
N	Number of molecules adsorbed
P	Pressure [bar]
PSA	Pressure Swing Adsorption
q	Uptake [mol/kg MOF]
q_{st}	Isosteric heat of adsorption [kJ/mol]
R	Gas constant [8.314 kPa m^3/ kmol K]
r_{ij}	Distance between two atoms, *i* and *j*
$S_{1/2}$	Selectivity of 1 over 2
SAP	Swing Adsorption Processes
T	Temperature [K]
TOT	total
TSA	Temperature Swing Adsorption
U	Total potential energy of a system [kJ/mol]

$U_{i/j}$	Potential energy between a pair of atoms *i* and *j* [kJ/mol]
V	Volume
VSA	Vacuum Swing Adsorption
W	Work [J]
WC_i	Working capacity [mol/kg MOF]
X	Purity
x	Mole fraction of a component in the adsorbed phase
y	Mole fraction of a component in the gas phase
Δ	Difference
ΔH	Enthalpy
ε_{LJ}	Lennard-Jones potential [kJ/mol]
η	Efficiency
ρ	MOF density [kg/m^3]
σ_{ij}	Lennard-Jones potential diameter [Å]
ϵ	Voidage of bed
Φ	Correction factor
Θ	Rotation angle
q	Atom charge

10. REFERENCES AND NOTES

[1] Yang H, Xu Z, Fan M, Gupta R, Slimane RB, Bland AE et al. Progress in carbon dioxide separation and capture: a review. J Environ Sci, **2008**, 20:14–27.

[2] Sabouni, R.; Kazemian, H.; Rohani, S. Carbon dioxide capturing technologies: a review focusing on metal oganic framework materials (MOFs), Environmental Science and Pollution Research, **2014**, 21 (8), 5427–5449.

[3] Rackley SA. Carbon capture and storage. ButterworthHeinemann/Elsevier, Burlington, **2010.**

[4] Luis, P. . Use of monoethanolamine (MEA) for CO2 capture in a global scenario: Consequences and alternatives. Desalination, **2016,** 380, 93-99.

[5] Douglas, A., & Tsouris, C. . Separation of CO2 from flue gas: a review. Separation Science and Technology, **2005**, 40(1-3), 321-348.

[6] Olajire AA. CO2 capture and separation technologies for end-ofpipe applications—a review. Energy, **2010**, 35:2610–2628

[7] Ebner AD, Ritter JA. State-of-the-art adsorption and membrane separation processes for carbon dioxide production from carbon dioxide emitting industries. Sep Sci Technol, **2009**, 44:1273–1421

[8] Ruthven, D. M. Principles of adsorption and adsorption processes. John Wiley & Sons, **1984**.

[9] Dąbrowski, A. Adsorption—from theory to practice. Advances in colloid and interface science, **2001**, 93(1-3), 135-224.

[10] IUPAC. International Union of pure and applied chemistry. https://iupac.org (accessed May 2, 2019).

[11] Sarabadan, S. Adsorptive air separation behavior on silver exchanged ETS-10 Typed Molecular Sieves, **2011**. PhD Thesis.

[12] Tejero, J. Apunts de Disseny de Catalitzadors. Màster d'Enginyeria Química. Universitat de Barcelona. **2015**

[13] Rouquerol, J.; Rouquerol, F.; Llewellyn, P.; Maurin, G.; Sing, K; Adsorption by powders and porous solids, **1998**.

[14] Reporting Physisorption Data for Gas/Solid Systems with Special Reference to the Determination of Surface Area and Porosity, IUPAC Commission on Colloid and Surface Chemistry Including Catalysis, Pure Appl. Chem., 57 (1985) 603; Recommendations for the Characterization of Porous Solids, IUPAC Commission on Colloid and Surface Chemistry, Pure Appl. Chem., 66, **1994**, 1311.

[15] Brunauer, S.; Emmet, P.H.; Teller, E. Adsorption of gases in multimolecular layers, **1938.**

[16] Prats, H., Bahamon, D., Alonso, G., Giménez, X., Gamallo, P., & Sayos, R. Optimal Faujasite structures for post combustion CO2 capture and separation in different swing adsorption processes. Journal of CO2 Utilization, **2017**, 19, 100-111.

[17] Prats, H., Bahamon, D., Gimenez, X., Gamallo, P., & Sayos, R. Computational simulation study of the influence of faujasite Si/Al ratio on CO2 capture by temperature swing adsorption. Journal of CO2 Utilization, **2017**, 21, 261-269.

[18] Tarka TJ, Ciferno JP, Gray ML, Fauth D. CO capture systems using amine enhanced solid sorbents. Presented at the Fifth Annual Conference on Carbon Capture & Sequestration. Alexandria, VA, USA, **2006**, pp152.

[19] Bansal, R. C., & Goyal, M. Activated carbon adsorption. CRC press, **2005.**

[20] Li, J. R., Kuppler, R. J., & Zhou, H. C. Selective gas adsorption and separation in metal–organic frameworks. Chemical Society Reviews, **2009**, 38(5), 1477-1504.

[21] Zhao, Y.; Song, Z.; Li, X.; Sun, Q.; Cheng, N.; Lawes, S.; Sun, X. Metal organic frameworks for energy storage and conversion. Energy Storage Materials, **2016**, 2, 35-62.

[22] Glover, T. G., Peterson, G. W., Schindler, B. J., Britt, D., & Yaghi, O. MOF-74 building unit has a direct impact on toxic gas adsorption. *Chemical Engineering Science*, **2011**, *66*(2), 163-170.

[23] Shi, B.; Al-Dadah, R.; Mahmoud, S.; Elsayed, A.; Elsayed, E. CPO-27 (Ni) Metal-Organic Framework Based Adsorption System for Auto-motive Air Conditioning. Applied Thermal Engineering, **2016,** 106-325-333.

[24] Wang, H.; Qu, Z. G.; Zhang, W.; Chang, Y. X.; He, Y. L. Experimental and numerical of CO2 adsorption Ni/DOBDC metal-organic framework. Applied Thermal Engineering, **2014,** 73(2), 1501-1509.

[25] Olajire AA. CO2 capture and separation technologies for end-ofpipe applications—a review. Energy, **2010**, 35:2610–2628.

[26] Figueroa JD, Fout T, Plasynski S, McIlvried H, Srivastava RD. Advances in CO2 capture technology—The U.S. Department of Energy's Carbon Sequestration Program. Int J Greenh Gas Control, **2008**, 2:9–20

[27] Liu, J.; Wang, Y.; Benin, A. I.; Jakubczak, P.; Willis, R. R.; LeVan, M. D. CO2/H2O Adsorption Equilibrium and Rates on Metal-Organic Frameworks: HKUST-1 and Ni/DOBDC. Langmuir, **2010**, 26 (17), 14301–14307.

[28] Hedin, N.; Andersson, L.; Bersgtröm, L.; Yan, J.; Adsorbent for the post-combustion capture of CO2 using rapid temperature swing or vacuum swing adsorption. Applied Energy, **2013**, 104, 418-433.

[29] Raventós, M., Duarte, S., & Alarcón, R. Application and possibilities of supercritical CO2 extraction in food processing industry: an overview. Food Science and Technology International, **2002**, 8(5), 269-284.

[30] Ecobiogas. http://www.ecobiogas.es (accessed 6 May 2019).

[31] Otto, A., Grube, T., Schiebahn, S., & Stolten, D. Closing the loop: captured CO 2 as a feedstock in the chemical industry. Energy & environmental science, **2015,** 8(11), 3283-3297.

[32] Lokhorst, A., & Wildenborg, T. Introduction on CO2 Geological storage-classification of storage options. Oil & gas science and technology**, 2005**, 60(3), 513-515.

[33] Frenkel, D.; Smit, B.; Understanding Molecular Simulations from algorithms to applications, **2002.**

[34] Erucar, I.; Keskin, S. High CO2 Selectivity of an Amine-Functionalized Metal Organic Framework in Adsorption-based and membrane-based Gas Separations. Ind. Eng. Chem. Res., **2013**, 52 (9), 3462–3472.

[35] González, J.; Demontis, P.; Baldovino, G.; Métodos deterministas y estocásticos aplicados al estudio de materiales microporosos, **2010**.

[36] Torrens, I.M. Interatomic potentials. Academic Press, New York. **1972**.

[37] Allen, M.P.; Tildesley, D.J.; Computer Simulation of Liquids, **1987**

[38] Gutiérrez, G.; Elementos de simulación computacional, **2001**.

[39] Rubinstein, R. Y., & Kroese, D. P. Simulation and the Monte Carlo method (Vol. 10). John Wiley & Sons, **2016.**

[40] Becker, T. M.; Heinen, J.; Dubbeldam, D.; Lin, L.; Vlught, T. J. H. Polarizable Force Fields for CO2 and CH4 Adsorption in M-MOF-74. J. Phys. Chem. C, **2017**, 121,4659.

[41] Potoff, J.J.; Siepmann, J. I. Vapor–liquid equilibria of mixtures containing alkanes, carbon dioxide, and nitrogen, AIChE J., **2001**, 47, 1676–1682.

[42] Ketko, M. H.; Kamath, G.; Potoff, J. J. Development of an optimized intermolecular potential for sulfur dioxide, J. Phys. Chem. C, **2011**, 115 (17), 4949–4954.

[43] C.W. Skarstrom, Method and apparatous for fractionating gaseous mixtures by adsorption, US Patent 2944627, **1960**.

[44] Y. Chung, B.K. Na, H.K. Song, Short-cut evaluation of pressure swing adsorption systems, Comput. Chem. Eng. 22, **1998**, S637–S640.

[45] A.L. Chaffee, G.P. Knowles, Z. Liang, J. Zhang, P. Xiao, P.A. Webley, CO2 capture by adsorption: materials and process development, Int. J. Green. Gas Control.1, **2007**, 11–18.

[46] L. Riboldi, O. Bolland, J.M. Ngoy, N. Wagner, Full-plant analysis of a PSA CO2 capture unit integrated in coal-fired power plants: post- and pre-combustion scenarios, Energy Procedia 63, **2014**, 2289–2304.

[47] Tur, M. Molecular Modelling of Industrial Gases Separation by Adsorption on Metal-Organic Frameworks. Universitat de Barcelona, **2018**.

[48] Queen, W. L.; Hudson, M. R.; Bloch, E. D.; Mason, J. A.; Gonzalez, M. I.; Lee, J. S.; Gygi, D.; Howe, J. D.; Lee, K.; Darwish, T. A.; et al. Comprehensive Study of Carbon Dioxide Adsorption in the Metal–organic Frameworks M2(DOBDC) (M = Mg, Mn, Fe, Co, Ni, Cu, Zn). Chem. Sci**. 2014**, 5(12), 4569–4581.

[49] Surendra, K. C., Takara, D., Hashimoto, A. G., & Khanal, S. K. Biogas as a sustainable energy source for developing countries: Opportunities and challenges. Renewable and Sustainable Energy Reviews, **2014**, 31, 846-859.

APPENDIX

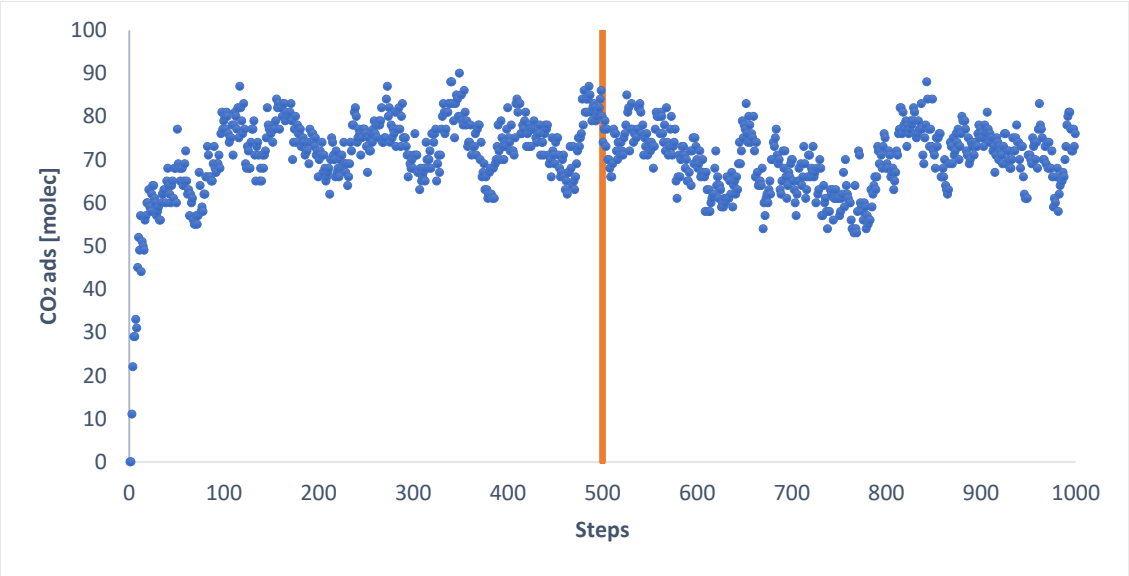

Figure A1. Example of simulation in GCMC method: CO_2 molecules adsorbed at 1 bar in pure CO_2.

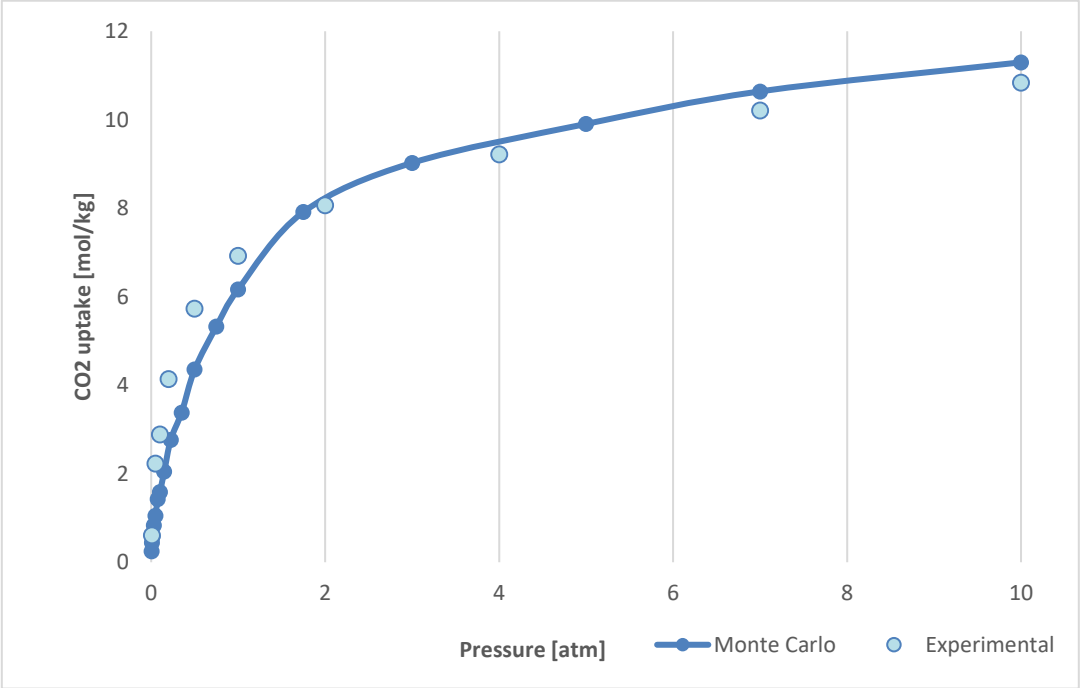

Figure A2. CO_2 isotherm at 298 K. Results obtained from [47] compared with experimental data from Queen et al [48].

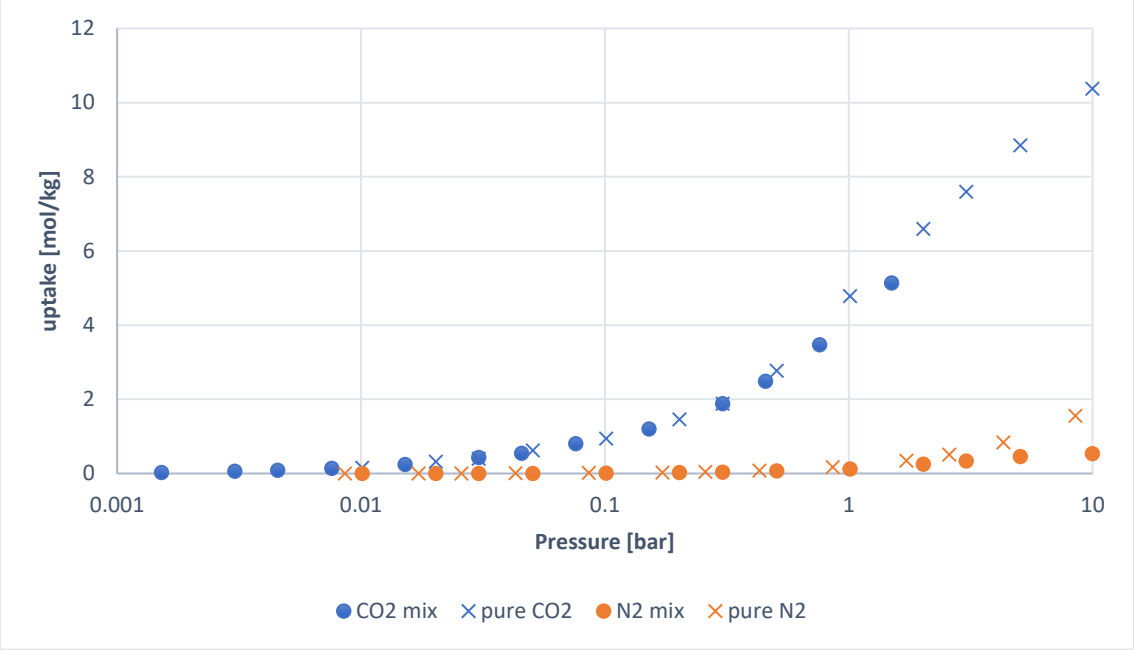

Figure A3. Uptake comparation of pure CO_2, pure N_2 and post-combustion gases (T=313K).

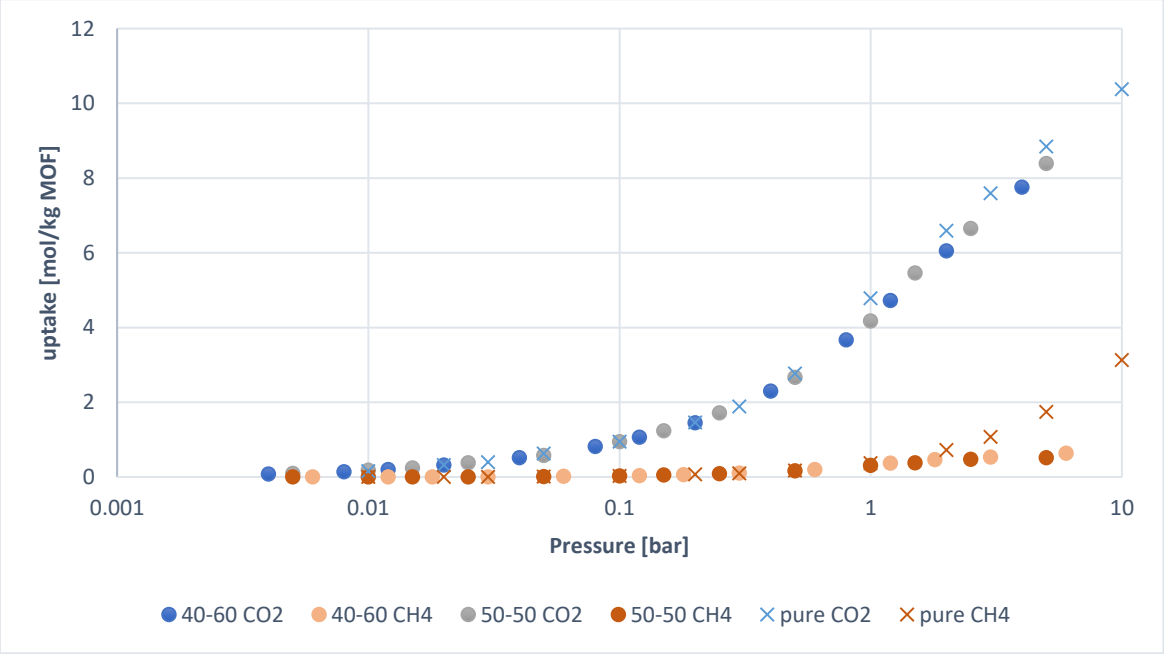

Figure A4. Uptake comparation of pure CO2, pure CH4 and biogas gases (40:60, 50:50).

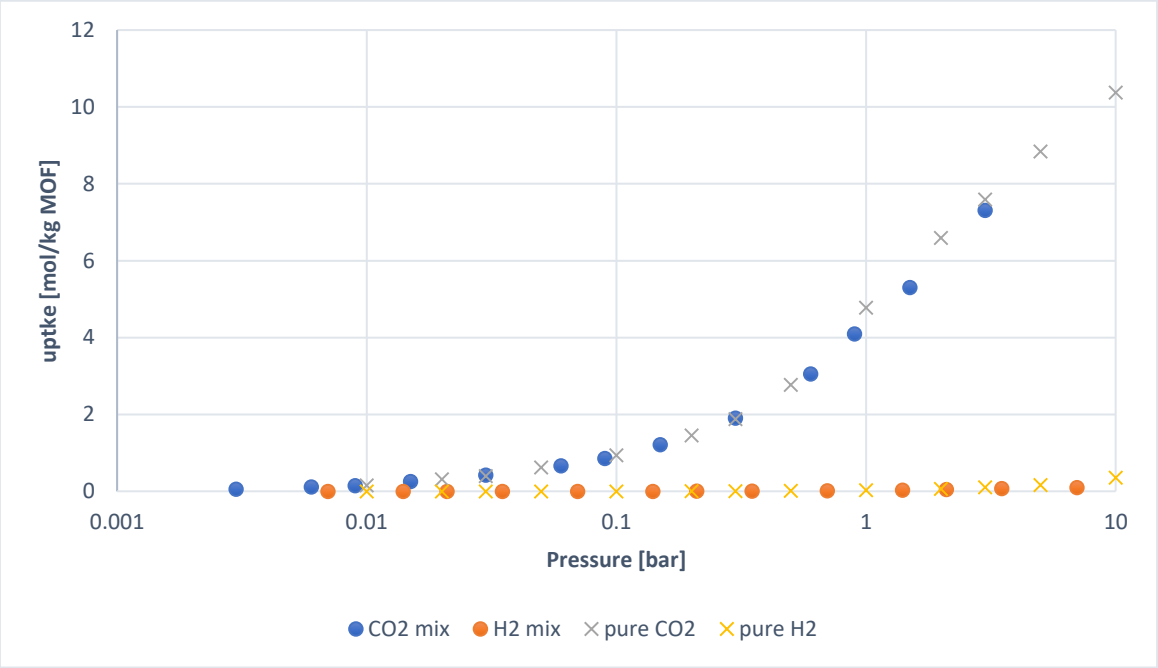

Figure A5. Uptake comparation of pure CO2, pure H2 and syngas gases.